Article

Neuron

Septal Cholinergic Neuromodulation Tunes the Astrocyte-Dependent Gating of Hippocampal NMDA Receptors to Wakefulness

Highlights

- D-serine availability at hippocampal synapses fluctuates with wakefulness
- Septal cholinergic signaling determines D-serine levels, via α7nAChRs
- α7nAChRs directly located on astrocytes drive the vesicular release of D-serine
- An α7nAChR modulator used in schizophrenia clinical trials augments NMDAR gating

Authors

Thomas Papouin, Jaclyn M. Dunphy, Michaela Tolman, Kelly T. Dineley, Philip G. Haydon

Correspondence

philip.haydon@tufts.edu

In Brief

Astrocytes release gliotransmitters at synapses, but how this impacts synaptic physiology over time is unclear. Focusing on the gliotransmitter D-serine, Papouin et al. demonstrate that astrocytes tune synaptic properties to the ongoing brain state, a concept they term "contextual guidance."

Papouin et al., 2017, Neuron *94*, 840–854
May 17, 2017
http://dx.doi.org/10.1016/j.neuron.2017.04.021

CellPress

CellPress

Neuron
Article

Septal Cholinergic Neuromodulation Tunes the Astrocyte-Dependent Gating of Hippocampal NMDA Receptors to Wakefulness

Thomas Papouin,[1] Jaclyn M. Dunphy,[2] Michaela Tolman,[2] Kelly T. Dineley,[3] and Philip G. Haydon[1,4,*]
[1]Department of Neuroscience, Tufts University School of Medicine, Boston, MA 02111, USA
[2]Neuroscience Program, Tufts Sackler School of Graduate Biomedical Sciences, Boston, MA 02111, USA
[3]Department of Neurology, University of Texas Medical Branch, Galveston, TX 77555, USA
[4]Lead contact
*Correspondence: philip.haydon@tufts.edu
http://dx.doi.org/10.1016/j.neuron.2017.04.021

SUMMARY

The activation of the N-methyl D-aspartate receptor (NMDAR) is controlled by a glutamate-binding site and a distinct, independently regulated, co-agonist-binding site. In most brain regions, the NMDAR co-agonist is the astrocyte-derived gliotransmitter D-serine. We found that D-serine levels oscillate in mouse hippocampus as a function of wakefulness, in vitro and in vivo. This causes a full saturation of the NMDAR co-agonist site in the dark (active) phase that dissipates to sub-saturating levels during the light (sleep) phase, and influences learning performance throughout the day. We demonstrate that hippocampal astrocytes sense the wakefulness-dependent activity of septal cholinergic fibers through the α7-nicotinic acetylcholine receptor (α7nAChR), whose activation drives D-serine release. We conclude that astrocytes tune the gating of synaptic NMDARs to the vigilance state and demonstrate that this is directly relevant to schizophrenia, a disorder characterized by NMDAR and cholinergic hypofunctions. Indeed, bypassing cholinergic activity with a clinically tested α7nAChR agonist successfully enhances NMDAR activation.

INTRODUCTION

N-methyl D-aspartate receptors (NMDARs) play a direct role in many aspects of brain physiology, such as learning and memory. They are also involved in a variety of disorders, and a hypofunction of synaptic NMDAR signaling is the main hypothesis for the etiology of schizophrenia, a chronic and severe mental disorder that affects 2.6 million adults in the United States (Javitt, 2015; Moghaddam and Javitt, 2012; Ripke et al., 2014). Activation of NMDARs requires the presence of a co-agonist, in addition to their agonist glutamate (Johnson and Ascher, 1987; Kleckner and Dingledine, 1988), and D-serine plays this role in many brain regions, in particular the hippocampus (Henneberger et al., 2010; Papouin et al., 2012). Because D-serine is thought to be a gliotransmitter released by astrocytes (Bergersen et al., 2012; Henneberger et al., 2010; Martineau et al., 2013; Panatier et al., 2006), an interesting corollary is that astrocytes could regulate the availability of D-serine at synapses to control NMDAR independently of neuronal activity. However, because the conditions and stimuli that govern D-serine release are unidentified, it is still unknown whether astrocytes can modulate the concentrations of D-serine they supply to NMDARs under certain conditions of brain activity.

Brain disorders often shed light on the physiological pathways at play in the healthy brain, and our current understanding of the etiology of schizophrenia points to a possible link between brain cholinergic activity and NMDAR co-agonist gating. D-serine levels are lowered in the plasma of schizophrenic patients (Hashimoto et al., 2003; Bendikov et al., 2007), and many human mutations associated with schizophrenia result in a hypofunction of NMDAR co-agonist binding site by decreasing its affinity or by directly impairing D-serine availability (Labrie et al., 2012; Ma et al., 2013; Ripke et al., 2014). In parallel, a dysregulation of the cholinergic system is a hallmark of schizophrenia (Freedman, 2014; Javitt, 2015), and recent clinical trials aimed to improve cognitive symptoms of schizophrenic patients with cholinergic modulators (Javitt, 2015).

Cholinergic neurons in the medial septum send scattered projections to cortical regions where their activity results in ambient levels of acetylcholine (ACh), or extracellular ACh "tone," involved in long-range and long-lasting effects (Teles-Grilo Ruivo and Mellor, 2013). In these regions, the ACh tone fluctuates with changes in vigilance state: the highest levels are found during active wakefulness and the lowest during slow-wave sleep (Marrosu et al., 1995; Lee et al., 2005; Zant et al., 2016). Interestingly, ACh is known to influence NMDAR activity and NMDAR-dependent functions (Kirkwood et al., 1999; Lin et al., 2014; Markram and Segal, 1990; Yang et al., 2013; Zappettini et al., 2014), and activates intracellular signaling in astrocytes through various ACh receptors (AChRs) (Hirase et al., 2014; Sharma and Vijayaraghavan, 2001; Shen and Yakel, 2012; Takata et al., 2011). Combined with evidence that ACh can promote D-serine synthesis and/or release (Lin et al., 2014; Singh et al., 2013; Takata et al., 2011), these data point to a link between vigilance state-dependent cholinergic activity and NMDAR co-agonist gating via astrocytic D-serine.

This hypothesis greatly aligns with the most recent view of astrocyte function. Indeed, the time course of astrocytic activity is several orders of magnitude slower than neurons (Vardjan et al., 2016). This makes astrocytes good candidates to receive, integrate, and relay information about the neuromodulatory state of the brain, such that their impact on neuronal and brain function has become increasingly relevant in the scope of behavioral states (Chen et al., 2012; Ding et al., 2013; Hirase et al., 2014; Panatier et al., 2006; Schmitt et al., 2012; Paukert et al., 2014). This is supported by evidence that astrocytes are exquisite sensors of neuromodulators, such as norepinephrine and acetylcholine, that are involved in sensory modalities and vigilance states (Ding et al., 2013; Lee et al., 2005; Paukert et al., 2014; Pinto et al., 2013; Hirase et al., 2014; Navarrete et al., 2012; Sharma and Vijayaraghavan, 2001; Shen and Yakel, 2012; Takata et al., 2011). Here we used a variety of in vivo and in vitro approaches to examine fluctuations of endogenous D-serine availability throughout the day and their link with cholinergic activity. We found that the wakefulness-dependent cholinergic activity from the medial septum governs astrocytic release of D-serine via the activation of astrocytic α7nAChRs, thus tuning the gating of hippocampal NMDARs to wakefulness. We also show that bypassing the endogenous cholinergic activity with an α7nAChR partial agonist, used in a phase III clinical trial for the treatment of schizophrenia, successfully enhances D-serine levels, highlighting the relevance of our findings to the therapeutic approach of schizophrenia.

RESULTS

D-Serine Availability Oscillates over the 24 hr Period

To determine whether there are daily fluctuations in D-serine levels, we first performed extracellular recordings of synaptic NMDAR-mediated field excitatory post-synaptic potentials (NMDA-fEPSPs) in the stratum radiatum of acute hippocampal slices (Figures S1A–S1C; STAR Methods). Slices were obtained at different Zeitgeber times (ZTs; ZT0 is the onset of light) across the 24 hr period, and the endogenous occupancy of the NMDAR co-agonist-binding site was determined by adding a saturating concentration of exogenous D-serine (50 μM; Figures S1A–S1D). We found that the effect of D-serine application was highly dependent on the time of day at which slices were obtained (Figure 1A; $F(6,50) = 9.889$, $p < 10^{-6}$, one-way ANOVA; Figures S1E–S1G). Exogenous D-serine failed to potentiate NMDA-fEPSPs at ZT0 (Figure 1A and B; $t(9) = 0.87$, $p = 0.407$, paired Student's t test), indicating that the NMDAR co-agonist site was already fully saturated, but produced significant ($p < 0.01$, paired Student's t tests) and increasing effects in slices obtained from ZT1 through ZT13 (Figures 1A and S1G; ZT1, 17% ± 2.4%; ZT2, 20.9% ± 3.3%; ZT6, 25.7% ± 3.6%; ZT13, 28.7% ± 5.8%). In the dark (active) phase, the occupancy of NMDARs progressively increased as revealed by weakening effects of D-serine application from ZT13 to ZT23 (Figures 1A and 1B; $p = 0.001$, Bonferroni post hoc test; Figures S1A–S1G). Importantly, these fluctuations were not due to changes in the co-agonist site's affinity for D-serine since the subunit composition of NMDARs, assessed with the GluN2A- and GluN2B-NMDAR-specific antagonists zinc (250 nM) and Ro25-6981 (2 μM), respectively, did not change over the 24 hr period (Figure 1C; $F(2,18) = 0.298$ and $F(2,22) = 0.649$, $p > 0.05$, one-way ANOVAs). Together, these data suggest that the amount of endogenous co-agonist available to NMDARs fluctuates across the 24 hr period.

Since D-serine is the endogenous co-agonist of NMDARs at CA3-CA1 synapses (Papouin et al., 2012), we directly assessed extracellular D-serine levels (Figures 1D and 1E; STAR Methods). Hippocampal slices obtained at ZT0 and ZT6 were incubated in aCSF for 90 min, and D-serine concentration in this conditioned medium (CM) was then measured using amperometric biosensors (Dale et al., 2005). D-serine amounts, both absolute (−32%) and normalized to the protein content of incubated tissue (−27%), were significantly lower in the CM obtained from ZT6 slices (Figures 1F and 1G; $p < 0.05$, Student's t tests), supporting the existence of daily fluctuations of free extracellular D-serine levels in hippocampal slices. We concluded that the oscillations in the occupancy of NMDAR co-agonist site are caused by oscillations in the endogenous concentration of D-serine. Therefore, the "saturation index" is used thereafter as a proxy for the amount of D-serine available to synaptic NMDARs (ZT6, 0.800 ± 0.020; ZT0, 0.985 ± 0.018; $t(18) = 6.84$, $p < 0.0001$, Student's t test; Figure 1H). It is directly calculated from the increase in NMDA-fEPSP slope caused by exogenous D-serine (Figures S1B and S1C; STAR Methods) and represents the baseline occupancy of NMDAR co-agonist site: the higher the concentrations of endogenous D-serine, the higher the saturation index.

D-Serine Fluctuations Are Driven by Wakefulness, Not Circadian Rhythms

D-serine is present at saturating levels at the end of the dark (active) phase, rapidly declines to non-saturating levels in the light (sleep) phase, and progressively builds up again through the dark phase (Figure 1), seemingly following daily levels of wakefulness (Figure S2). To understand whether D-serine oscillations are governed by wakefulness and activity or by an intrinsic 24 hr circadian rhythm, mice were subjected to enforced wakefulness (EW) between ZT0 and ZT2 before hippocampal slices were obtained (STAR Methods; Figures S2A and S2B). This should be without effect on D-serine supply if it is determined by the time of day through a circadian mechanism. However, EW should prevent the rapid decline of D-serine at the onset of the light phase if D-serine supply is driven by wakefulness. We found that after 2 hr of EW, the saturation index was significantly greater than that measured at ZT2 from undisturbed mice (Figures 1A and 1I; $t(18) = 3.97$, $p = 0.0009$, Student's t test). This effect was only transient and the saturation index returned to control levels after 4 hr of rest following EW (Figures 1A and 1I). Since prolonging wakefulness through the light phase can maintain saturating levels of D-serine, we asked whether favoring active exploratory behavior with enriched environment housing (EEH) could accelerate D-serine accumulation during the dark phase (STAR Methods; Figures S2A and S2C). We found that EEH increased wakefulness in the dark phase, especially during the first 6 hr (Figures S2A and S2C), and that the saturation index measured in ZT18 slices was enhanced in mice kept in EEH (Figures 1A and 1J; $t(14) = -3.2$, $p = 0.0064$, Student's t test), indicating that increased activity accelerated the buildup of D-serine. Together, these results demonstrate that oscillations in D-serine availability at CA3-CA1 synapses are not driven by

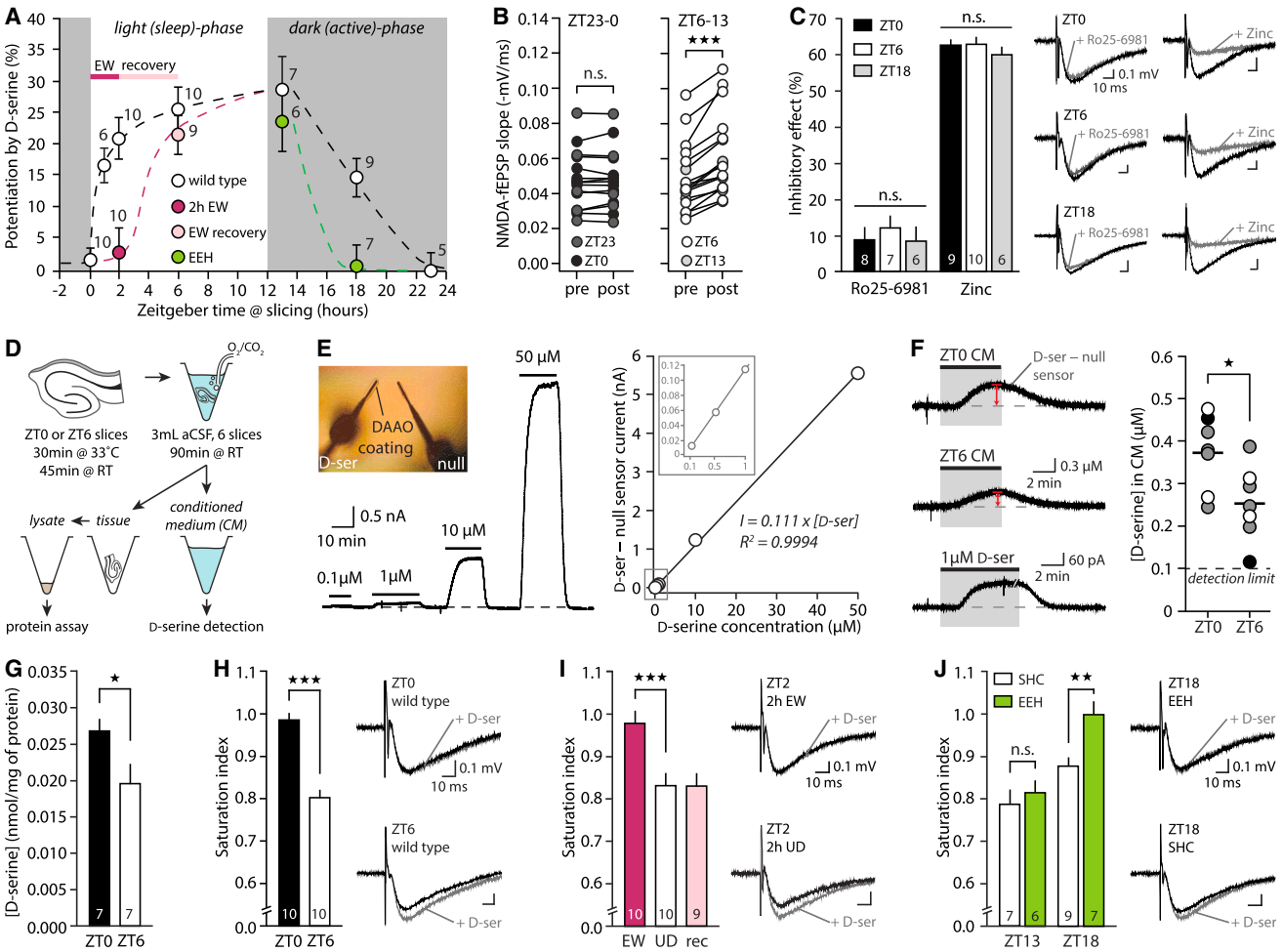

Figure 1. Daily Oscillations of D-Serine Availability Are Driven by Wakefulness

(A) Effect of D-serine application on NMDA-fEPSPs in slices obtained at different Zeitgeber times (ZTs) from WT mice, mice subjected to enforced-wakefulness (EW), EW mice after 4 hr of recovery, and mice in enriched environment housing (EEH). Dotted lines are provided as visual guides.

(B) Individual slopes of NMDA-fEPSPs before (pre) and after (post) D-serine application, at indicated ZTs.

(C) Inhibitory effect of the GluN2B-NMDAR antagonist Ro25-6981 (2 µM) and GluN2A-NMDAR antagonist zinc (250 nM) at ZT0, ZT6, and ZT18 and illustrative traces.

(D) Schematic showing the collection of conditioned medium (CM).

(E) Calibration of the D-serine biosensors showing their linearity, including for sub-micromolar D-serine (right inset).

(F) D-serine measurements in ZT0 and ZT6 CM. Each circle indicates the value obtained from one animal. Color code shows "pairs" of ZT0 and ZT6 CMs run on the same set of biosensors. Horizontal bars represent average.

(G) Average D-serine concentration in CM normalized to the weight of tissue incubated (mg of protein).

(H–J) Saturation index of NMDARs at ZT0 and ZT6 (H); at ZT2 in slices from EW mice, undisturbed (UD) mice, or EW mice after 4 hr of recovery (rec) (I); and at ZT13 and ZT18 in slices from mice housed in EEH or in standard home cages (SHC) (J). Pooled data are shown as mean ± SEM.

See also Figures S1 and S2.

circadian rhythms but instead follow a mechanism wherein wakefulness and activity promote the accumulation of D-serine while rest/sleep favors its clearance.

D-Serine Levels Fluctuate with Wakefulness In Vivo

To validate these findings in a more physiological setting, we carried out in vivo micro-dialysis from area CA1 of the hippocampus of freely behaving mice from ZT0 to ZT6, while video monitoring their activity during the entire 6 hr of micro-dialysis (Figures 2A and 2B; STAR Methods). The absolute D-serine and L-serine concentration in the dialysate was then determined through high-performance liquid chromatography (HPLC) on a C18 column using concentration standards (Figure 2C; STAR Methods). The average concentration of D-serine (1.8 ± 0.3 µM) and L-serine (13.3 ± 1.2 µM) measured across mice was very similar to that found in the literature (Figure 2D; Fukushima et al., 2004). However, we also observed that the concentration of D-serine measured in the dialysates was significantly correlated to the percentage of time mice spent active during the 6 hr of micro-dialysis ($p = 0.0018$, one-tailed Pearson correlation test;

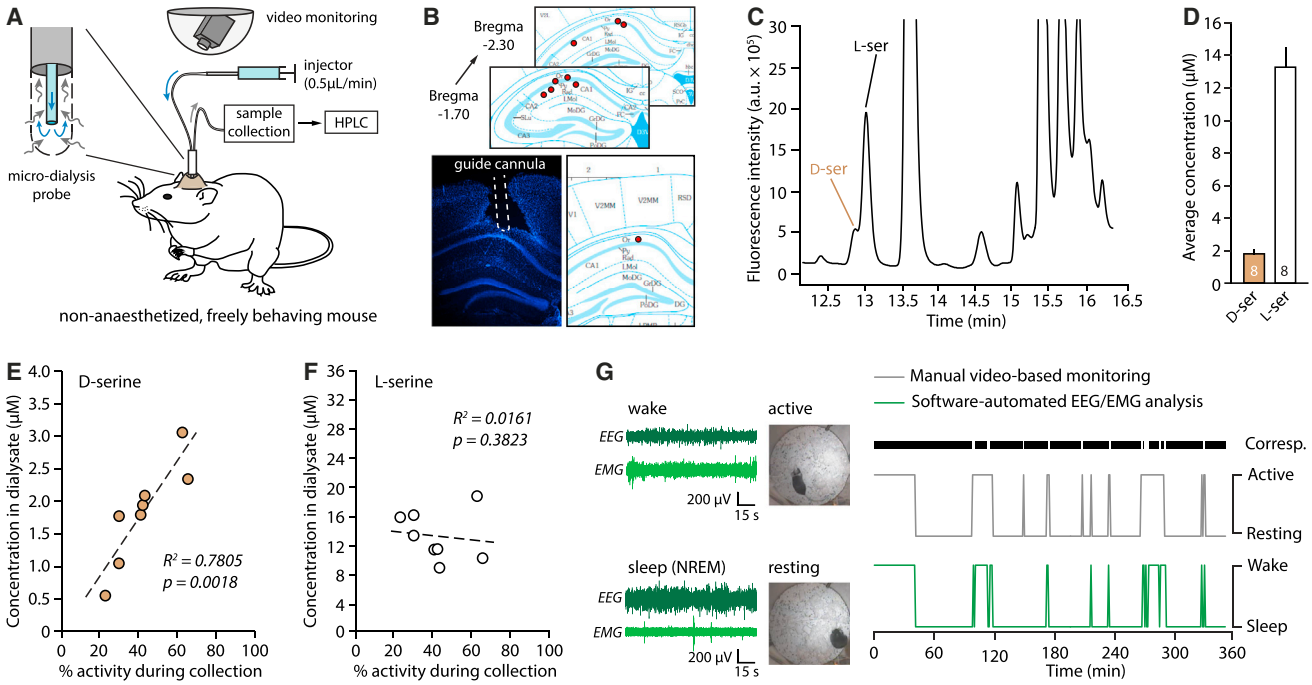

Figure 2. Wakefulness-Dependent Fluctuations of D-Serine Concentration In Vivo

(A) Experimental set up for in vivo micro-dialysis and video monitoring from ZT0 to ZT6.

(B) Histological targeting of micro-dialysis probes on the Allen Brain Atlas (top) determined on DAPI-stained hippocampal section (bottom).

(C) HPLC chromatogram showing L-serine and D-serine peaks.

(D) Average D-serine and L-serine concentrations in eight different mice.

(E) Individual D-serine concentrations in dialysates as a function of the average percentage of time the mouse spent active during micro-dialysis.

(F) Same as (E) for L-serine.

(G) Left: video snapshots and EEG/EMG traces representing the active/resting state and the wake/sleep state. Right: actograms (6 hr) of the same mouse obtained using video-based or EEG/EMG scoring of activity/wakefulness. The black horizontal bar indicates the sections of correspondence (corresp.) between the two scoring systems.

See also Figure S3.

Figure 2E). The lowest D-serine concentrations were found in the dialysate of mice that spent 70%–80% of the time nested and immobile, while the highest amounts were measured in mice with levels of activity greater than 60%. This correlation was specific for D-serine since L-serine levels were not correlated to activity ($p = 0.3823$; Figure 2F), and a correspondence test independently validated that actograms obtained from video monitoring are a faithful proxy of wakefulness measured by EEG/EMG recordings (Figure 2G; 95.2% agreement, kappa value = 0.876; see Figure S3A). Together, these experiments indicate that D-serine levels measured in vivo with micro-dialysis reflect the overall wake/sleep history of the mouse during the dialysate collection. This conclusively demonstrates that D-serine concentration fluctuates with wakefulness in the mouse hippocampus, varying more than 5-fold between rest (~0.5 µM) and wakefulness (3 µM), thus nearly spanning the entire range of NMDAR co-agonist site sensitivity (Paoletti et al., 2013).

Daily D-Serine Fluctuations Impact Learning and Memory

In order to evaluate the significance of such endogenous D-serine oscillations to behavior, we probed an NMDAR-dependent learning and memory assay. We examined contextual fear memory, a task that relies on hippocampal NMDARs (Matus-Amat et al., 2007; Schenberg and Oliveira, 2008) in which mice learn to associate foot shocks with the context where they are delivered. Mice were trained at different ZTs and re-exposed to the context 24 hr later, and the amount of time they spent freezing was measured (Figure 3A). Mice trained at ZT0 and tested 24 later had greater levels of freezing (+62%) compared to mice trained at ZT6 and tested 24 hr later ($p = 0.0017$, Bonferroni post hoc test; Figures 3B and 3C), revealing a more efficient formation of hippocampal memory at ZT0 consistent with higher levels of D-serine (Figures 1G and 1H). The immediate response to shocks (Figure 3B) was similar in all groups, indicating that there were no differences in sensitivity/aversion to the electrical stimuli during training. As expected for this task, the difference between the ZT0 and ZT6 groups was also context dependent: mice tested in a different context (context B; STAR Methods) had low and identical levels of freezing (Figure 3D; $t(22) = 1.07$, $p = 0.2962$, Student's t test).

Mice are less active during the light phase, which could diminish their capability to explore and encode the environment and its aversive nature at ZT6. To test if the reduced memory at ZT6 was attributable to weaker acquisition, mice were trained at ZT0 or ZT6 and tested 1 hr later in the original context. Both

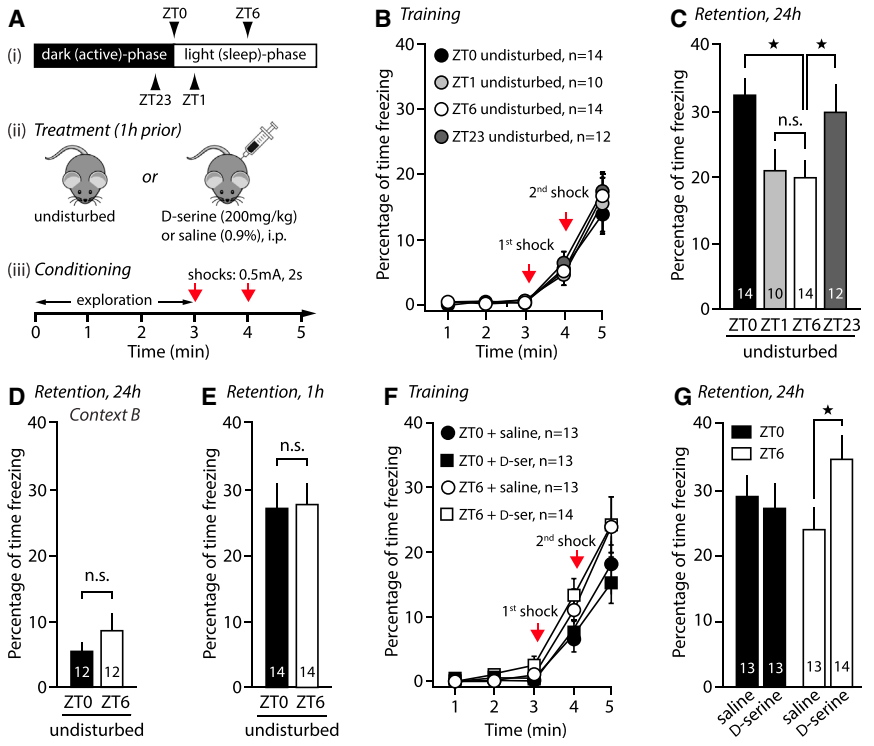

Figure 3. Oscillations in NMDAR Occupancy Impact Learning and Memory

(A) Schematic of the timing, injection, and training paradigm for contextual fear conditioning.

(B) Immediate freezing responses of undisturbed mice during training at different ZTs.

(C) Freezing response 24 hr later for mice trained in (B).

(D) Freezing response in a different context, 24 hr after training at ZT0 and ZT6.

(E) Freezing response of mice 1 hr after training at ZT0 and ZT6.

(F) Immediate freezing responses of mice during training at ZT0 and ZT6, 1 hr after i.p. injections of saline or D-serine.

(G) Freezing responses, 24 hr later, for mice trained in (F).

All panels show mean ± SEM. See also Figure S3.

groups showed strong freezing levels and performed identically (Figure 3E; $t(25) = 0.14$, $p = 0.8897$), indicating that mice can acquire and retrieve short-term contextual memory equally, regardless of the ZT at training.

ZT6-trained mice had 6 hr of light phase remaining after training whereas ZT0-trained mice had almost 12 hr (Figure 3A). Because memory consolidation occurs during episodes of sleep after training (Maingret et al., 2016), we considered this confounding factor by assessing the performance of mice trained at ZT1 (when D-serine is low in slices, similar to ZT6; Figure 1) and tested 24 hr later (~11 hr of light phase remaining after training, like at ZT0). This group showed reduced levels of freezing that were identical to the ZT6 group (Figures 3B and 3C; $p = 0.846$, Bonferroni post hoc test), indicating that enhanced memory in the ZT0 group was not the result of a greater time spent in light phase after training. Finally, to explore the possibility that mice performed better at ZT0 because they cued the task with light onset, a group of mice was trained and tested in the dark phase (ZT23, a time when D-serine levels are high in slices, similar to ZT0; Figure 1). Handling of mice was carried out under red light, except for the dim lighting of the contextual chamber. Levels of freezing in this group were similar to the ZT0 group and greater than the ZT6 group (Figures 3B and 3C; $p = 0.0410$, Bonferroni post hoc test), ruling out the possibility that ZT0-trained mice used light onset as a learning strategy.

Overall, the magnitude of contextual fear memory oscillates from ZT0 to ZT23 (Figure 3C; $F(3,47) = 4.26$, $p = 0.0088$, one-way ANOVA) and recapitulates both the saturation level of NMDARs in slices and the finding that in vivo D-serine levels depend on overall wakefulness. This suggested that daily oscillations of hippocampal D-serine contribute to this behavioral effect. If true, increasing brain D-serine with intraperitoneal (i.p.) administration (200 mg/kg; Figure S3B; Fukushima et al., 2004) should improve fear memory at ZT6, but not at ZT0, since D-serine is naturally saturating at ZT0, but not at ZT6. In agreement with this assumption, D-serine treatment (200 mg/kg intraperitoneally 1 hr prior to training; Figure 3A) significantly increased the percentage of freezing in the ZT6 group compared to saline ($t(26) = -2.16$, $p = 0.0402$), whereas it failed to improve freezing levels at ZT0 (Figures 3F and 3G; $t(24) = 0.41$, $p = 0.685$). That D-serine-treated mice performed identically to saline-treated littermates at ZT0 also indicates that D-serine did not enhance overall motor or cognitive skills. Together, these results indicate that the oscillations in D-serine levels occur over a range of concentrations that is relevant to behavior, such as learning and memory.

Astrocytes Are the Source of Activity-Dependent D-Serine Supply

D-serine is considered a gliotransmitter, but it can also be found in neurons (see Balu et al., 2014). Therefore, we examined the contribution of astrocytes to daily oscillations of D-serine availability by assessing NMDAR saturation index in slices obtained from astrocyte-specific dnSNARE mice (Figure 4A; Pascual et al., 2005). In these mice, the tetO-dnSNARE:GFAP-tTA transgenic construct drives the expression of the cytoplasmic domain of the vesicular protein VAMP2 selectively in astrocytes (astrocyte-specific *GFAP* promoter), following removal of doxycycline (Dox) from the diet (STAR Methods). This impairs the formation of the SNARE complex in astrocytes by a dominant-negative effect, reducing by 91% the exocytotic release of gliotransmitters, including D-serine (Pascual et al., 2005; Sultan et al., 2015). It should be noted that, in agreement with the vast majority of the astroglial literature that used dnSNARE mice, a systematic examination performed by two independent investigators in both area CA1 and CA3 failed to identify a single eGFP-expressing neuron among 5,884 and 5,887 neurons counted in 24 stacks from 5 different animals (Figures S4A–S4D). This careful

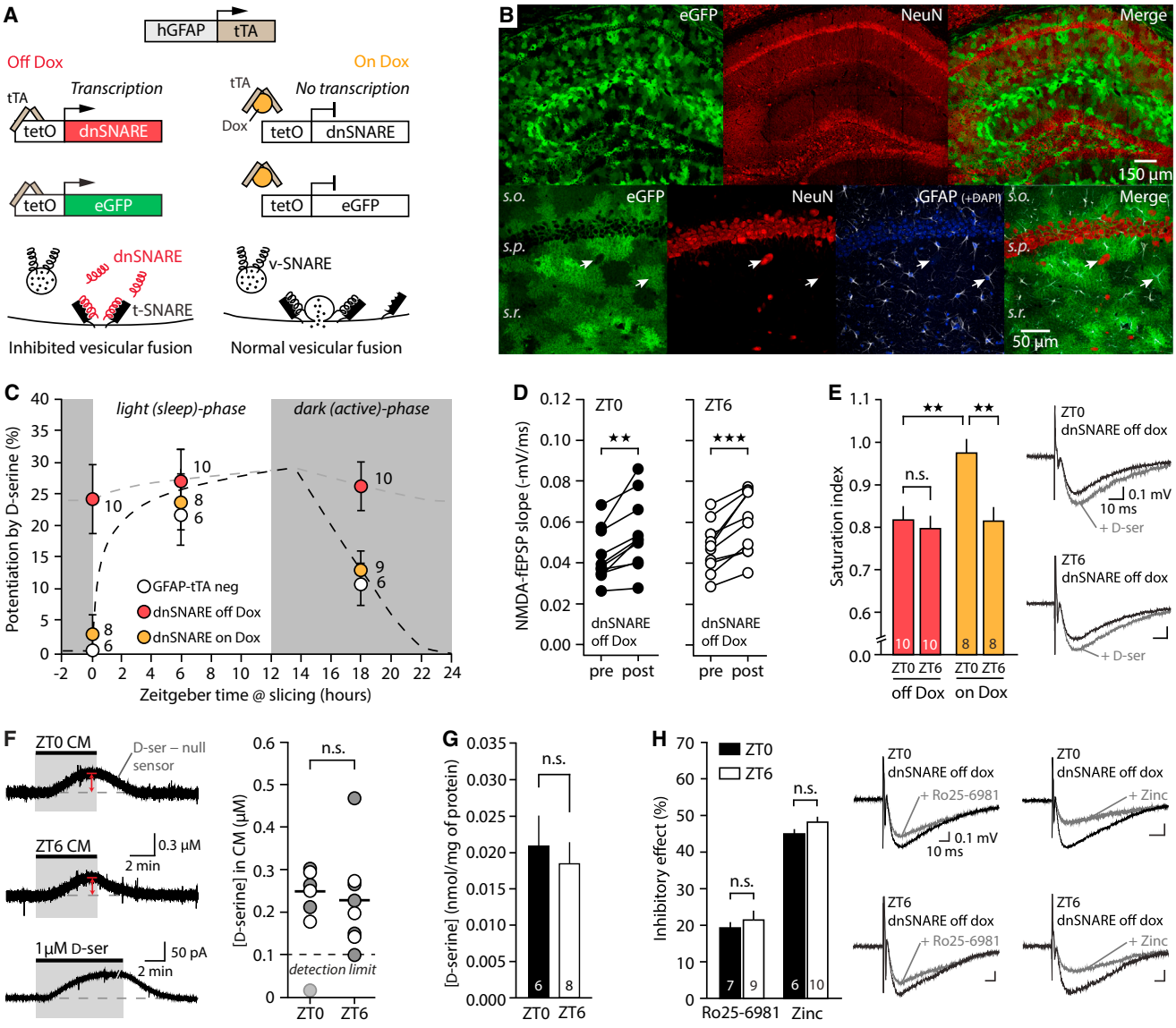

Figure 4. Inhibition of SNARE-Mediated Vesicular Release in Astrocytes Abolishes D-Serine Oscillations

(A) Schematic of conditional astrocyte-specific expression of dnSNARE and eGFP transgenes in dnSNARE mice. Animals are raised on Dox until weaning.

(B) Upper panels: composite confocal images showing the mosaic expression of the eGFP reporter in hippocampal astrocytes of a dnSNARE mouse kept off Dox for 8 weeks after weaning (stitch of 20 images 20×, NA 0.75). Lower panels: confocal (40×) images of DAPI nuclear staining, eGFP fluorescence, and NeuN (neuronal) and GFAP (astrocytic) immunoreactivity (so, stratum oriens; sp, stratum pyramidale; sr, stratum radiatum). Arrows show an eGFP-negative neuron and an eGFP-positive astrocyte.

(C) Effect of D-serine application on NMDA-fEPSPs in slices obtained from GFAP-tTA-negative animals (single gene control) and dnSNARE mice off or on Dox, at different ZTs. Dotted lines serve as visual guides.

(D) Individual slopes of NMDA-fEPSPs before (pre) and after (post) D-serine application at ZT0 and ZT6 in slices from dnSNARE mice off Dox.

(E) Saturation index at ZT0 and ZT6 in slices from dnSNARE mice off or on Dox.

(F) D-serine measurements in ZT0 and ZT6 CM from dnSNARE mice off Dox.

(G) Average D-serine concentration in CM normalized to the weight of tissue incubated (mg of protein).

(H) Effect of the GluN2B-NMDAR antagonist Ro25-6981 and the GluN2A-NMDAR antagonist zinc on NMDA-fEPSPs in ZT0 and ZT6 slices from dnSNARE mice off Dox. Pooled data are shown as mean ± SEM.

See also Figure S4.

assessment is in striking contrast to and refutes the claims from Fujita et al. (2014), and confirms the cell specificity of transgene expression in dnSNARE mice (Figures 4A and 4B). In slices from dnSNARE mice off Dox, we found that the effect of exogenous D-serine on NMDA-fEPSPs was independent of the time of day (Figure 4C; $F(2,28) = 0.085$, $p = 0.918$, one-way ANOVA), in

contrast with slices from single gene controls (GFAP-tTA negative) in which the same oscillations found in wild-type (WT) mice were observed ($F(2,15) = 8.666$, $p = 0.0032$). In slices obtained at ZT0 from dnSNARE mice off Dox, D-serine significantly augmented NMDA-fEPSPs (Figure 4D; $t(9) = 4.39$, $p = 0.0017$, paired Student's t test; see Figures S4E and S4F) and the resulting saturation index was identical to that found at ZT6 (Figure 4E; $t(18) = 0.44$, $p = 0.665$, Student's t test). Additionally, NMDAR subunit composition was the same in ZT0 and ZT6 slices (Figure 4H; $p > 0.05$, one-way ANOVAs) and amperometric measurements revealed similar levels of D-serine in ZT0 and ZT6 slices from dnSNARE mice off Dox (Figures 4F and 4G; $p > 0.05$, Student's t tests). Importantly, reintroducing Dox into the diet for a month to suppress transgene expression ("dnSNARE on Dox"; STAR Methods) was sufficient to restore daily oscillations of D-serine (Figure 4C; $F(2,24) = 8.042$, $p = 0.0024$, one-way ANOVA) and the differential saturation at ZT0 and ZT6 (Figure 4E; $t(14) = 3.52$, $p = 0.0034$, Student's t test). Together, these data demonstrate that D-serine oscillations rely on astrocytic SNARE-dependent supply of D-serine during the dark phase.

D-serine and its synthesizing enzyme serine racemase are also present in neurons (Balu et al., 2014; and see Wolosker and Radzishevsky, 2013), suggesting a potential contribution of neurons to D-serine supply. This has prompted the proposal of an "L-serine/D-serine shuttle" wherein (1) astrocytes provide L-serine to neurons, (2) D-serine is synthesized in neurons from L-serine, and (3) neurons release D-serine (Wolosker and Radzishevsky, 2013). According to this view, an alternative interpretation of our results would be that neuronal D-serine release is impaired in dnSNARE mice due to the lack of L-serine supply from astrocytes. However, providing exogenous L-serine (20 μM, 45 min) did not restore the saturation index in dnSNARE slices at ZT0 (Figures S4G and S4H), indicating that the expression of the dnSNARE transgene directly prevented the release of D-serine, not L-serine, by astrocytes.

Cholinergic Tone Drives Wakefulness-Dependent D-Serine Release from Astrocytes

In addition to being tightly correlated with vigilance states (Lee et al., 2005; Marrosu et al., 1995; Zant et al., 2016), cholinergic signaling potentiates NMDAR activity and modulates NMDAR-dependent functions (Kirkwood et al., 1999; Lin et al., 2014; Markram and Segal, 1990; Yang et al., 2013; Zappettini et al., 2014). ACh also elicits intracellular Ca^{2+} signaling in astrocytes through muscarinic receptors (Takata et al., 2011), α4β2- and α4β4-nAChR (Gahring et al., 2004), or α7nAChRs (Sharma and Vijayaraghavan, 2001; Shen and Yakel, 2012) and can promote D-serine release or synthesis (Lin et al., 2014; Singh et al., 2013; Takata et al., 2011). Therefore, we hypothesized that ACh is the signal that tunes D-serine levels to wakefulness and tested whether cholinergic agonists can enhance the saturation index of NMDARs in ZT6 slices (Figure 5A). Application of a broad AChR agonist, carbamylcholine (Carba; Figure 5E), caused a full saturation of NMDARs (Figure 5A; $p < 10^{-7}$ versus control, Bonferroni post hoc tests) that persisted in the presence of atropine ($p = 0.899$ versus Carba), suggesting the involvement of nicotinic (nAChRs), rather than muscarinic, receptors. The most abundant nAChRs expressed by hippocampal astrocytes in C57BL/6 mice are α4β2- and α4β4-nAChRs (Gahring et al., 2004), but Carba still caused a full saturation of NMDARs in the presence the α4β4- and α4β2-nAChR antagonist DHβE ($p = 0.889$). In contrast, we found that the effect of Carba was prevented by the α7nAChR antagonist MLA (Figure 5A; $p < 10^{-9}$), in line with observations that α7nAChR activation promotes NMDAR activity (Lin et al., 2014; Yang et al., 2013; Zappettini et al., 2014) and favors D-serine release (Singh et al., 2013). As expected from this finding, the α7nAChR selective agonist AR-R17779 (AR-R) alone elicited a full saturation of NMDARs ($p < 10^{-8}$ versus control), which was attenuated by the co-application of MLA ($p < 10^{-4}$ versus AR-R). Importantly, stimulation of α7nAChRs did not change the subunit composition of NMDARs (Figure S5A), indicating that it did not change NMDAR affinity for D-serine but rather increased extracellular D-serine levels. Finally, in line with studies reporting the presence of α7nAChRs on astrocytes (Duffy et al., 2011; Gahring et al., 2004; Sharma and Vijayaraghavan, 2001; Shen and Yakel, 2012; Zhang et al., 2014), we found that application of neither Carba nor AR-R altered the saturation index in slices from dnSNARE mice off Dox (Figure 5A; $F(2,24) = 0.0031$, $p = 0.997$, one-way ANOVA), suggesting that α7nAChR stimulation elicits D-serine release from astrocytes.

That the stimulation of α7nAChRs elevates D-serine levels in ZT6 slices suggested that the saturating levels of D-serine found at ZT0 could be due to a basal activation of α7nAChRs. We tested this hypothesis and found that incubations of ZT0 slices with MLA for 60 min or more reduced NMDAR saturation index to a level similar to that normally found at ZT6 (Figures 5B and 5C; $t(19) = 8.78$, $p < 10^{-6}$, Student's t test), while it had no effect in slices obtained at ZT6 ($t(16) = 0.8$, $p = 0.4354$), or in ZT0 slices from dnSNARE mice off Dox ($t(18) = 0.66$, $p = 0.5176$). Altogether, these results indicate that the daily oscillations in NMDAR co-agonist site occupancy are driven by the wakefulness-dependent endogenous activation of α7nAChRs upstream of astrocytic exocytosis.

Similar to ACh, the activity of noradrenergic neurons is phased to vigilance state (Aston-Jones and Bloom, 1981), and norepinephrine (NE) directly impacts astrocyte Ca^{2+} activity through α1 adrenergic receptor α1AR (Ding et al., 2013; Paukert et al., 2014). We thus asked whether adrenergic activity could also influence the release of D-serine and found that the saturation index in ZT6 slices was altered neither by the presence of NE nor by the specific α1AR agonist methoxamine (Figure 5A; $p > 0.05$, Bonferroni post hoc tests). Similarly, we found that oscillations in D-serine availability do not originate from changes in purinergic tone across the 24 hr period (Figures S5C–S5G), demonstrating that wakefulness-dependent release of hippocampal D-serine is selectively influenced by cholinergic neuromodulation.

Our findings suggest a direct and specific mechanistic link between α7nAChR activity and NMDAR co-agonist site, which is highly relevant in the context of schizophrenia. Indeed, the α7nAChR is the target of several therapeutics that have been taken into clinical trials to improve cognitive deficits associated with schizophrenia (Freedman, 2014; Beinat et al., 2015; Javitt, 2015). Yet the mechanism underlying their beneficial effect is ill defined. We asked whether the most recent of them, EVP-6124 (FORUM Pharmaceuticals, phase III clinical trial

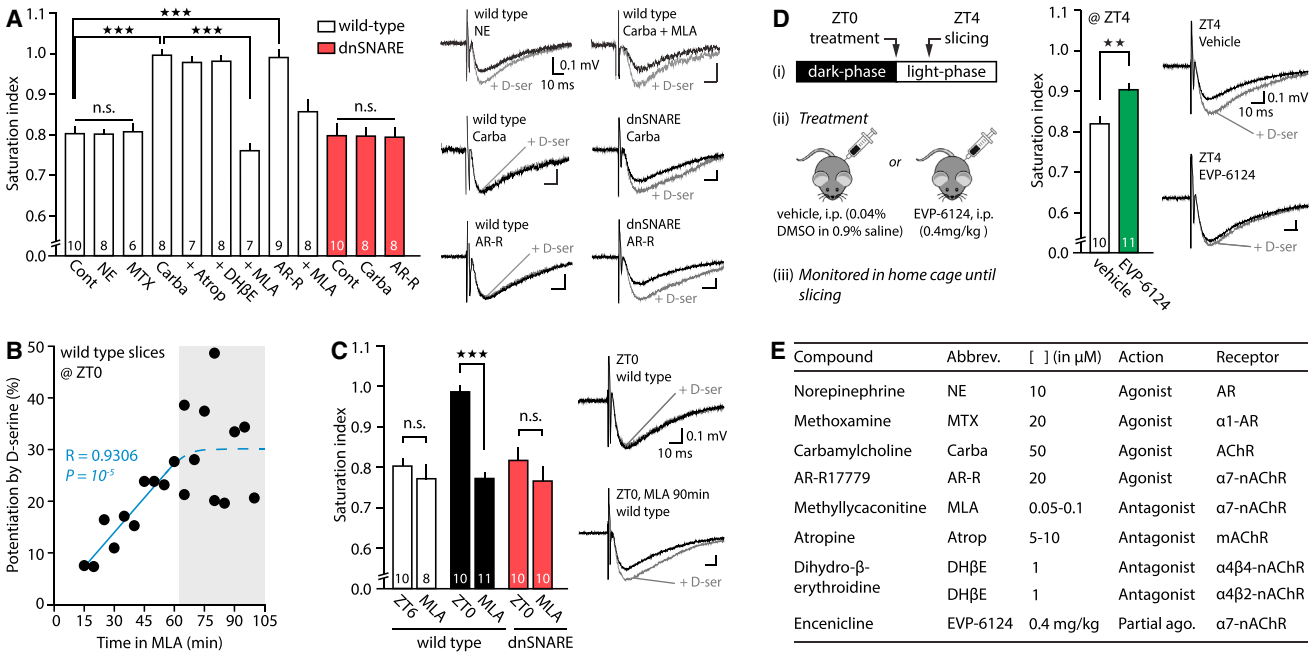

E

Compound	Abbrev.	[ ] (in μM)	Action	Receptor
Norepinephrine	NE	10	Agonist	AR
Methoxamine	MTX	20	Agonist	α1-AR
Carbamylcholine	Carba	50	Agonist	AChR
AR-R17779	AR-R	20	Agonist	α7-nAChR
Methyllycaconitine	MLA	0.05-0.1	Antagonist	α7-nAChR
Atropine	Atrop	5-10	Antagonist	mAChR
Dihydro-β-erythroidine	DHβE	1	Antagonist	α4β4-nAChR
	DHβE	1	Antagonist	α4β2-nAChR
Encenicline	EVP-6124	0.4 mg/kg	Partial ago.	α7-nAChR

Figure 5. Endogenous Cholinergic Signaling Controls D-Serine Availability across the 24 hr Period

(A) NMDAR saturation index in slices from WT and dnSNARE mice off Dox in the presence of adrenergic and cholinergic agonists/antagonists: norepinephrine (NE, 10 μM), α1AR agonist (MTX, 20 μM), AChR broad agonist (Carba, 50 μM), Carba and the muscarinic AChR antagonist atropine (+Atrop, 5–10 μM), Carba and the α4β2- and α4β4-nAChR antagonist DHβE (+DHβE, 1 μM), Carba and the α7nAChR antagonist MLA (+MLA, 50–100 nM), the α7nAChR agonist AR-R17779 alone (AR-R, 20 μM), and the combination of AR-R and MLA. See Figure 5E.

(B) Effect of MLA incubation on NMDA-fEPSPs potentiation by D-serine. Individual experiments are shown. Plateau effect is reached after 60 min incubation (gray area).

(C) Effect of MLA incubation (>60 min) on NMDAR saturation index in ZT0 and ZT6 slices from WT mice, and ZT0 slices from dnSNARE off Dox.

(D) Experimental set up for i.p. injections of EVP-6124 or vehicle in WT mice (left) and saturation index of NMDARs in slices obtained 4 hr later (right).

(E) Table summarizing the various compounds, their abbreviation, concentration, action, and target. Pooled data are shown as mean ± SEM.

See also Figure S5.

NCT01716975), was capable of enhancing NMDAR saturation index. Pharmacokinetic studies have shown that EVP-6124 reaches peak brain concentration 2 hr after administration and remains at effective concentrations for at least 4 hr (Prickaerts et al., 2012). We administered EVP-6124 to WT mice at ZT0 (0.4 mg/kg i.p single dose, as in Prickaerts et al., 2012; Figure 5D) and found that this significantly increased the saturation index of NMDARs in slices obtained 4 hr later ($t(19) = -3.37$, $p = 0.0032$, Student's t test) without causing prolonged wakefulness or enhanced locomotor activity (Figure S5B). This indicates that α7nAChR-targeting therapeutics can enhance NMDAR activity, likely via D-serine, raising the possibility that this is the mechanism of action that mediates their beneficial effects on cognition.

Activity of MS-DBB Cholinergic Fibers Drives the Release of D-Serine in the Hippocampus

To confirm that in situ release of endogenous ACh elicits D-serine elevations, we employed the ChAT-ChR2-eYFP BAC transgenic mouse line that selectively expresses channelrhodopsin (ChR2) in cholinergic fibers (Zhao et al., 2011). These mice display strong expression of ChR2-eYFP in the medial septum (MS) and the ventral diagonal band of Broca (DBB), where the cholinergic fibers innervating the hippocampus originate (Figures 6A and 6B; Teles-Grilo Ruivo and Mellor, 2013). In slices obtained at ZT4, optical stimulation of these fibers (460 nm, 10 s at 5 Hz/min for 15 min; STAR Methods; Figures 6C and S6B–S6F) caused a slow and long-lasting enhancement of NMDA-fEPSPs (Figure 6D; 24.0% ± 11.2% at 50–70 min [2] versus baseline [1], $t(9) = 2.82$, $p = 0.0198$, paired Student's t test) that was not observed in ChAT-*ChR2*$^{-/-}$ mice (Figure S6G). This effect was not observed on AMPA-fEPSPs either (Figure S6H), indicating that it was specific to NMDARs and not due to an overall increase in synaptic strength. Importantly, application of exogenous D-serine 70 min after optical stimulation had no further effect on NMDA-fEPSPs (Figures 6D; 2.8% ± 1.9% [3] versus [2], $t(9) = 1.57$, $p = 0.150$), revealing a full saturation of NMDARs caused by the optical stimulation. Consistently, optical stimulation was unable to potentiate NMDA-fEPSPs when delivered in the presence of saturating levels of exogenous D-serine (Figure 6E; $t(9) = -1.32$, $p = 0.217$), confirming that the release of endogenous ACh by direct stimulation of cholinergic fibers causes an increased occupancy of the NMDAR co-agonist site. To ask whether α7nAChR mediates this effect, we repeated the experiment in the presence of the α7nAChR antagonist MLA and found that optical stimulation failed to cause an increase of NMDA-fEPSPs (Figure 6F; $t(9) = 0.06$, $p = 0.953$) while subsequent D-serine application produced a standard 20.2% ± 4.2% potentiation

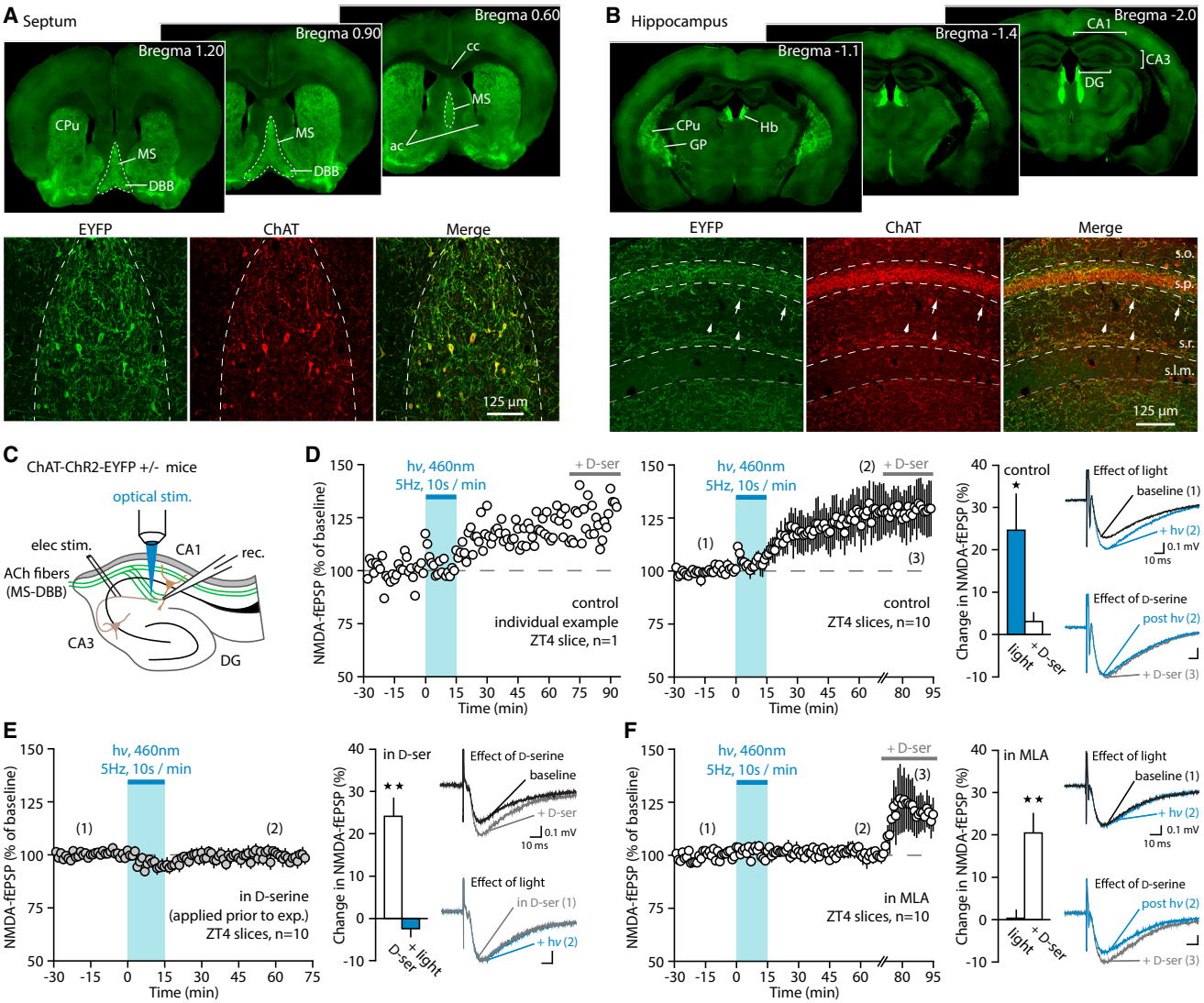

Figure 6. Cholinergic Volume Transmission Elicits a Long-Lasting Increase of NMDAR Co-agonist Site Occupancy

(A and B) Upper panels: eYFP fluorescence in the ventral diagonal band of Broca (DBB) and medial septum (MS) of ChAT-ChR2-eYFP mice (A), and their hippocampal projections (B). Anatomical structures are indicated for guidance and comparison with Zhao et al. (2011): caudate putamen (CPu), corpus callosum (cc), anterior commissure (ac), globus palidus (GP), habenula (Hb), and dentate gyrus (DG). Lower panels: 20× confocal images (maximum projection of three z-planes) of eYFP fluorescence and ChAT immunoreactivity in the MS (showing numerous cholinergic neurons; A) and the hippocampus (showing cholinergic fibers [arrowheads] and varicosities [arrows]; B).

(C) Set up of optogenetic experiments.

(D) Individual example (left) and average effect over time (right) of the optical stimulation of hippocampal cholinergic fibers on NMDA-fEPSPs. D-serine was applied at the end of the experiment to assess NMDAR saturation. Bar graphs show the average effect of light (2), compared to the baseline (1), and that of D-serine application (3), compared to the post-light plateau (2).

(E and F) Same as (D) in the presence of D-serine from the start of the experiment (E) or in the presence of MLA (F). In (E) the effect of D-serine is not shown on the time course. Data are shown as mean ± SEM.

See also Figure S6.

($t(9) = -4.44$, $p = 0.003$). This indicates that NMDARs had remained unsaturated following the optical stimulation and that α7nAchR indeed mediates D-serine elevations driven by ACh transmission. As a last validation, we reasoned that optical stimulation of cholinergic fibers should have no effect in slices obtained at ZT0, in which we found that both ACh and D-serine are already present at elevated levels. Accordingly, NMDA-fEPSPs remained unchanged following optical stimulation and D-serine application in ZT0 slices (Figure S6I).

We conclude that the release of endogenous ACh from MS-DBB cholinergic fibers scattered in the hippocampus elicits a long-lasting surge in D-serine concentration that causes a long-term potentiation of NMDAR activity, via the stimulation of α7nAChRs.

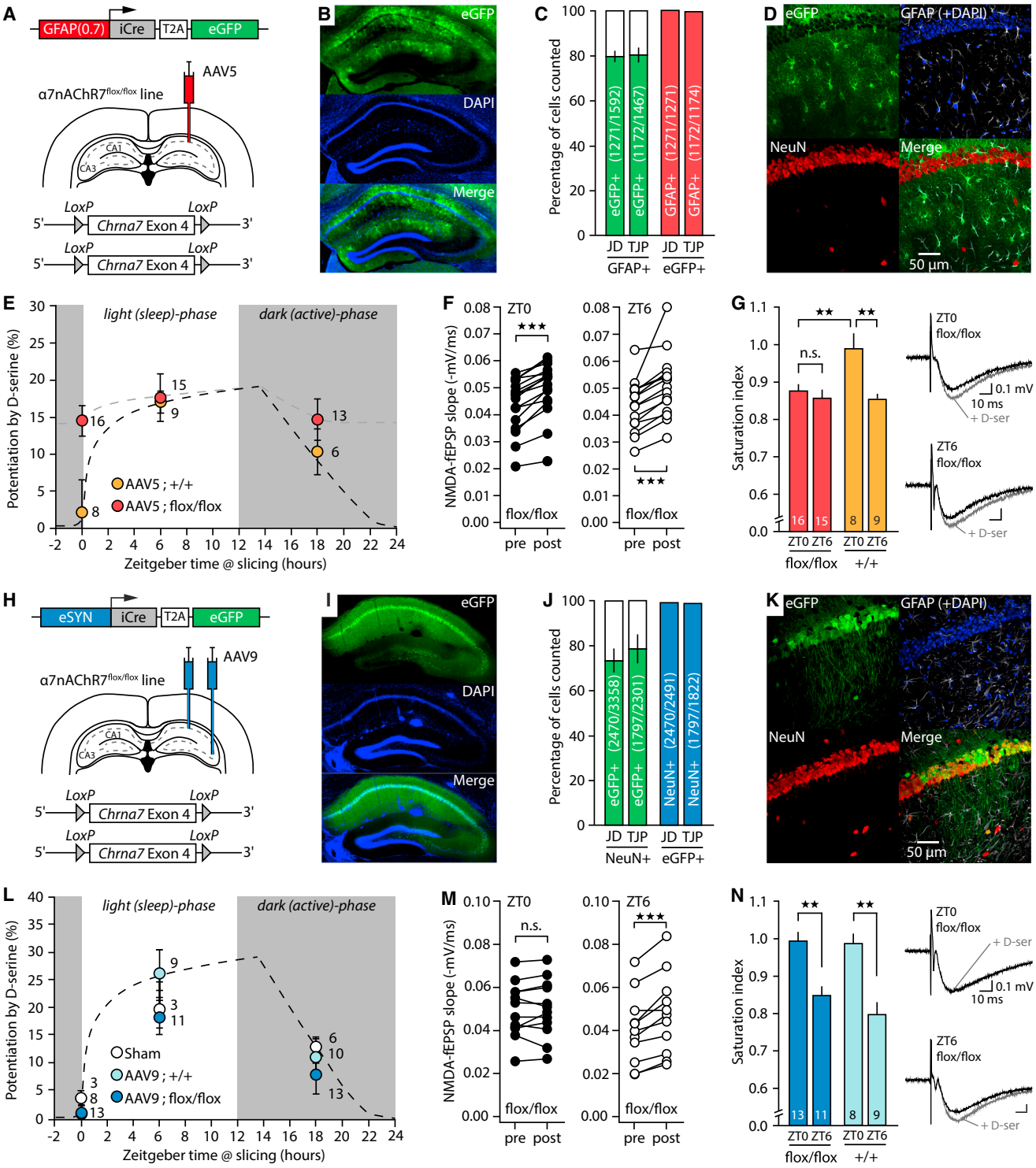

Figure 7. Astrocyte-Specific α7nAChR Knockout Abolishes D-Serine Oscillations

(A) Schematic of stereotaxic injections of Cre-encoding AAV5 virus in area CA1 of $\alpha7nAChR^{flox/flox}$ and $\alpha7nAChR^{+/+}$ littermates.

(B) eGFP fluorescence and DAPI staining in the hippocampus, 35 days after AAV5 injection.

(C) Percentage of GFAP+ cells (astrocytes) that are eGFP+ (expressing iCre) and percentage of eGFP+ cells that are GFAP+, counted by two independent investigators (J.D. and T.J.P.).

(D) Astrocyte specificity of the viral transduction: confocal (40×) images showing DAPI nuclear staining, eGFP fluorescence, NeuN (neuron), and GFAP (astrocyte) immunoreactivity.

(legend continued on next page)

Astrocytic α7nAChRs Mediate ACh-Driven D-Serine Oscillations

There have been increasing reports of the presence of α7nAChR on astrocytes (Duffy et al., 2011; Gahring et al., 2004) along with confirmations that such receptors are functional and play a signaling role (Sharma and Vijayaraghavan, 2001; Shen and Yakel, 2012). However, α7nAChRs are expressed by all cell types in the hippocampus, and while the RNA sequencing (RNA-seq) database shows expression in astrocytes, it is less abundant than in neurons (Gahring et al., 2004; Zhang et al., 2014). We thus asked whether α7nAChRs required for the wakefulness-dependent regulation of D-serine availability are located on astrocytes or neurons. We used mice in which exon 4 of *Chrna7* is floxed (α7nAChR$^{flox/flox}$; STAR Methods; Figure S7; Hernandez et al., 2014) and performed stereotaxic injections of adeno-associated viruses (AAVs) encoding Cre recombinase and GFP reporter. Mice were injected with an AAV5 encoding GFAP(0.7)-eGFP-T2A-iCre into area CA1 to selectively transduce astrocytes (Figure 7A), or with an AAV9 encoding eSYN-eGFP-T2A-iCre both in areas CA3 and CA1 to transduce neurons (Figure 7H). Mice were sacrificed at 35 ± 6 days post-injection and sections were immuno-stained for the astrocyte marker GFAP and the neuronal marker NeuN to confirm cell-type specificity of the transduction. As shown in Figures 7B–7D and 7I–7K, both the AAV5 and AAV9 viruses were highly selective for astrocytes and neurons, respectively.

NMDAR saturation index was assessed in slices from these animals, and these experiments were carried out blind to mouse genotype (STAR Methods). We found that the effect of D-serine application was independent of the time of day in slices from AAV5-α7nAChR$^{flox/flox}$ mice (Figure 7E; $F(2,42) = 0.4439$, $p = 0.6446$, one-way ANOVA) while it was ZT dependent in slices from AAV5-α7nAChR$^{+/+}$ mice ($F(2,20) = 5.5778$, $p = 0.0119$). At ZT0, D-serine applications yielded a significant increase of NMDA-fEPSPs in slices from AAV5-α7nAChR$^{flox/flox}$ (Figure 7F; $t(15) = 8.2$, $p < 10^{-5}$, paired Student's t test), revealing that the saturation index was impaired and similar to that found at ZT6 (Figure 7G; $t(29) = 0.8$, $p = 0.4278$, Student's t test). Thus, the loss of α7nAChR on astrocytes abolishes the oscillations in NMDAR saturation index. In contrast, the effect of D-serine application remained time-of-day dependent in AAV9-α7nAChR$^{flox/flox}$ slices (Figure 7L; $F(2,34) = 8.6824$, $p = 0.0009$, one-way ANOVA) in which NMDARs were fully saturated at ZT0 (Figure 7M; $t(12) = 0.91$, $p = 0.3825$; Figure 7N; $t(22) = 4.36$, $p = 0.0002$), indicating that the genetic deletion of the α7nAChR in pre- and postsynaptic neurons (as well as stratum radiatum interneurons) is without effect on the daily fluctuations of NMDAR co-agonist site occupancy. We conclude that astrocytic α7nAChRs are required for converting ACh drive into oscillations of NMDAR co-agonist site occupancy.

DISCUSSION

We demonstrate that by sensing wakefulness-dependent release of ACh through α7nAChRs, astrocytes modulate the amount of D-serine they provide to synaptic NMDARs throughout the day (Figure 8). There are three main consequences to this finding. First, this represents a new mechanism whereby NMDARs, and NMDAR-dependent functions, are controlled by vigilance state-dependent cholinergic activity through their co-agonist site. Second, we show that astrocytes are central to this mechanism: they locally shape synaptic properties to the ongoing brain activity by monitoring the neuromodulator environment, a new function we term "contextual guidance." Third, by linking cholinergic activity, α7nAChRs, astrocyte-derived D-serine, and NMDARs, this new pathway is greatly relevant to schizophrenia, and we demonstrate that the stimulation of α7nAChRs with a clinically tested drug (EVP-6124) is sufficient to enhance NMDAR function.

The degree of occupancy of the co-agonist binding site directly dictates the ability of NMDARs to be activated by glutamate (Kleckner and Dingledine, 1988). Since glutamate is fully saturating to NMDARs during synaptic transmission (Clements, 1996), D-serine availability is the limiting factor to NMDAR activation. We found that D-serine levels fluctuate in vivo as a function of wakefulness over a range of concentrations that spans NMDAR co-agonist site sensitivity. Therefore, the wakefulness-dependent control of D-serine we describe represents a new and major mechanism for the regulation of NMDAR activation throughout the day. It allows more robust NMDAR activity and higher learning capabilities during windows of higher behavioral alertness, in line with the well-documented memory-enhancing effect of nicotine. Such "on-demand" control of NMDAR activation also allows maintaining lower levels of hippocampal NMDAR activity during periods of rest, which could be relevant to synaptic downscaling and memory consolidation that occur during slow-wave sleep (Maingret et al., 2016). Overall, we predict that D-serine levels are regulated on demand in other brain regions as a function of their involvement in a specific behavioral task, vigilance state, or response to the hormonal status of the animal.

Behavioral states are intrinsically bound to neuronal population dynamics and to the activity of neuromodulator systems. For instance, states of wakefulness and attention coincide with bursting patterns of septal and/or locus coeruleus neurons and with volume transmission of NE and ACh (Aston-Jones and Bloom, 1981; Pinto et al., 2013; Lee et al., 2005; Zant et al., 2016). A significant body of evidence has now brought astrocytes into this scheme and suggests that astrocytes can sense brain states through volume transmission (Chen et al., 2012; Hirase et al., 2014; Navarrete et al., 2012; Paukert et al., 2014; Takata et al., 2011). Our study validates and extends this

(E) Effect of D-serine on NMDA-fEPSPs in slices obtained from AAV5-injected α7nAChR$^{flox/flox}$ and α7nAChR$^{+/+}$ littermates at different ZTs.
(F) Individual slopes of NMDA-fEPSPs before (pre) and after (post) D-serine application, at ZT0 and ZT6 in slices from AAV5-injected α7nAChR$^{flox/flox}$.
(G) Saturation index at ZT0 and ZT6 in slices from AAV5-injected α7nAChR$^{flox/flox}$ and α7nAChR$^{+/+}$ mice.
(H–N) Same as (A)–(G) for AAV9-injected animals. Note the neuronal specificity of the transduction. Sham, injected animals that showed no signs of virus transduction. Pooled data show mean ± SEM.
See also Figure S7.

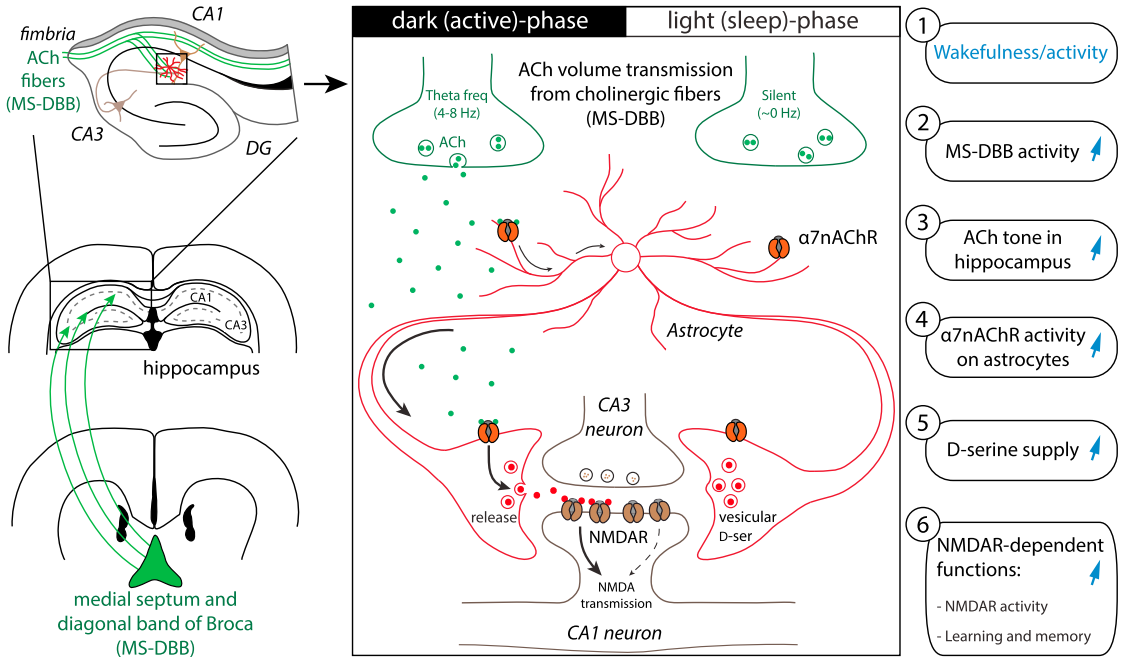

Figure 8. Cholinergic Transmission Tunes the Gating of NMDARs through Astrocyte-Dependent D-Serine Release

The medial septum and diagonal band of Broca (MS-DBB) send scattered cholinergic projections to the hippocampus. During active wakefulness (1), MS-DBB neurons fire in the theta frequency (2), which elicits the release of acetylcholine in the extracellular space (3). This cholinergic tone is sensed by astrocytes through α7nAChRs (4). This drives the vesicular release of astrocytic D-serine at synapses (5) to enhance NMDAR activity and NMDAR-dependent functions (6). The cessation of MS-DBB activity (during sleep and rest) suppresses the cholinergic-induced activation of α7nAChRs on astrocytes and reduces D-serine release.

emerging view by showing that hippocampal astrocytes sense wakefulness-dependent ACh neuromodulation and use this information to tune synaptic NMDAR activation via D-serine release. Based on similar reports that NE shapes astrocyte interactions with neurons in a context-dependent manner (Paukert et al., 2014), we postulate that the capability of hippocampal astrocytes to sense information about the brain state and use it to appropriately tune synaptic properties can be generalized to other neuromodulator systems and gliotransmission pathways. Therefore, we propose a new function for astrocytes wherein, by monitoring the neuromodulator environment and releasing appropriate gliotransmitters, astrocytes locally shape synaptic properties to the ongoing brain context, thus providing contextual guidance to synapses.

Multiple human mutations associated with schizophrenia point to a compromised function of the NMDAR co-agonist binding site, and this has become a leading hypothesis for the etiology and treatment of this disorder (Javitt, 2015; Moghaddam and Javitt, 2012; Ripke et al., 2014). This includes mutations that impair the synthesis, availability, or binding of D-serine such as mutations associated with *srr*, *DAO*, and *Grin1*, respectively coding for D-serine synthesizing enzyme serine racemase (SR), D-serine degrading enzyme D-amino acid oxidase (DAAO), and NMDAR GluN1 subunit that contains the co-agonist binding site (Labrie et al., 2012; Ma et al., 2013; Ripke et al., 2014). Similarly, the mutation of *Disc*-1 (disrupted-in-schizophrenia-1), a direct regulator of SR, is among the most notorious mutations associated with schizophrenia and causes a depletion of D-serine (Ma et al., 2013). In line with this genetic evidence, clinical studies reported decreased D-serine levels in the plasma of schizophrenic patients (Hashimoto et al., 2003; Bendikov et al., 2007), and administration of D-serine improves negative, positive, and general symptoms of schizophrenia (Kantrowitz et al., 2010). In parallel, the dysregulation of the cholinergic system has historically been a hallmark of schizophrenia (Javitt, 2015) and clinical attention is particularly focused on the α7nAChR. Indeed, α7nAChR modulators seem to significantly improve the cognitive deficits associated with schizophrenia in clinical trials (Beinat et al., 2015; Freedman, 2014; Javitt, 2015) even though no mechanisms have been proposed to explain such beneficial effects. Our work demonstrates that these two major hypotheses for the etiology and treatment of schizophrenia are mechanistically linked, via astrocytes. We show that impairing cholinergic signaling results in reduced D-serine availability and that, conversely, endogenous cholinergic activity can be bypassed with a clinically tested α7nAChR partial agonist to successfully enhance NMDAR activation. This provides mechanistic insights into the effects of clinically used α7nAChR modulators and highlights their potential to restore D-serine levels in schizophrenic patients, which is relevant when considering the nephrotoxicity of direct D-serine administration (Orozco-Ibarra et al., 2007). More importantly, our work places astrocytes at the center of this pathway, offering a new functional framework for the treatment of schizophrenia and opening the search for innovative approaches and targets to the field of glial biology.

In this context, the details of the signal transduction pathway linking the activation of α7nAChR to corresponding synaptic levels of D-serine will need to be defined. The α7nAChR is a highly Ca^{2+}-permeable ionotropic receptor and its activation triggers localized Ca^{2+} surges in astrocytes (Shen and Yakel, 2012; Sharma and Vijayaraghavan, 2001). Since D-serine release is SNARE and Ca^{2+} dependent (Henneberger et al., 2010; Martineau et al., 2013; Sultan et al., 2015), we presume that α7nAChR activation generates the optimal intracellular Ca^{2+} conditions that stimulate the release of D-serine-containing vesicles. Interestingly, evidence also exists that muscarinic AChRs induce an IP_3R2-mediated release of D-serine from astrocytes (Takata et al., 2011) or that TRPA1 channels regulate D-serine release (Shigetomi et al., 2013). Together, these results suggest that a complex and diversified set of local (membrane channels) and global (IP_3R2-dependent) Ca^{2+} sources control the release of D-serine. Our results also identify a pool of wakefulness-independent D-serine that remains unaffected by the blockade of α7nAChRs and SNARE-mediated vesicular release. This suggests the existence of a tonic source of D-serine that could be either astrocytic, but non-vesicular (Shigetomi et al., 2013), or neuronal (Wolosker and Radzishevsky, 2013). That multiple sources and routes of D-serine co-exist could constitute another interesting therapeutic target to control D-serine levels with, or independently of, wakefulness.

STAR★METHODS

Detailed methods are provided in the online version of this paper and include the following:

- KEY RESOURCES TABLE
- CONTACT FOR REAGENT AND RESOURCE SHARING
- EXPERIMENTAL MODEL AND SUBJECT DETAILS
  - Animals, housing and genotyping
  - Zeitgeber timescale
- METHOD DETAILS
  - Slice preparation
  - Field recordings
  - Optogenetics
  - Drugs
  - D-serine biosensor measurements in conditioned medium
  - Enforced-wakefulness and enriched-environment housing
  - In vivo microdialysis and HPLC
  - Wakefulness assessment, EEG-EMG recordings and analysis
  - Fear conditioning
  - Adeno-associated viruses and stereotaxic surgeries
  - Immunohistochemistry, fluorescence imaging and cell counting
- QUANTIFICATION AND STATISTICAL ANALYSIS

SUPPLEMENTAL INFORMATION

Supplemental Information includes seven figures and can be found with this article online at http://dx.doi.org/10.1016/j.neuron.2017.04.021.

A video abstract is available at http://dx.doi.org/10.1016/j.neuron.2017.04.021#mmc3.

AUTHOR CONTRIBUTIONS

T.P. conceptualized the study; designed, performed, and analyzed experiments; made the figures; and wrote the manuscript. J.M.D. and M.T. performed experiments. K.T.D. provided the $\alpha7nAChR^{flox/flox}$ mouse line. P.G.H. supervised the study, wrote the manuscript, and secured funding.

ACKNOWLEDGMENTS

This work was supported by a Philippe Foundation grant and a Human Frontier Science Program long-term fellowship (LT000010/2013) awarded to T.P., an NIH/NIMH F31 (MH106208) pre-doctoral fellowship awarded to J.M.D., an NIH/NINDS T32 Synapse Neurobiology Training Grant awarded to M.T., and two NIH/NINDS R01 grants (NS037585 and AA020183) awarded to P.G.H. P.G.H. is the founder of GliaCure.

Received: January 17, 2017
Revised: March 24, 2017
Accepted: April 12, 2017
Published: May 4, 2017

REFERENCES

Aston-Jones, G., and Bloom, F.E. (1981). Activity of norepinephrine-containing locus coeruleus neurons in behaving rats anticipates fluctuations in the sleep-waking cycle. J. Neurosci. *1*, 876–886.

Balu, D.T., Takagi, S., Puhl, M.D., Benneyworth, M.A., and Coyle, J.T. (2014). D-serine and serine racemase are localized to neurons in the adult mouse and human forebrain. Cell. Mol. Neurobiol. *34*, 419–435.

Beinat, C., Banister, S.D., Herrera, M., Law, V., and Kassiou, M. (2015). The therapeutic potential of α7 nicotinic acetylcholine receptor (α7 nAChR) agonists for the treatment of the cognitive deficits associated with schizophrenia. CNS Drugs *29*, 529–542.

Bendikov, I., Nadri, C., Amar, S., Panizzutti, R., De Miranda, J., Wolosker, H., and Agam, G. (2007). A CSF and postmortem brain study of D-serine metabolic parameters in schizophrenia. Schizophr. Res. *90*, 41–51.

Bergersen, L.H., Morland, C., Ormel, L., Rinholm, J.E., Larsson, M., Wold, J.F., Røe, A.T., Stranna, A., Santello, M., Bouvier, D., et al. (2012). Immunogold detection of L-glutamate and D-serine in small synaptic-like microvesicles in adult hippocampal astrocytes. Cereb. Cortex *22*, 1690–1697.

Chen, N., Sugihara, H., Sharma, J., Perea, G., Petravicz, J., Le, C., and Sur, M. (2012). Nucleus basalis-enabled stimulus-specific plasticity in the visual cortex is mediated by astrocytes. Proc. Natl. Acad. Sci. USA *109*, E2832–E2841.

Clements, J.D. (1996). Transmitter timecourse in the synaptic cleft: its role in central synaptic function. Trends Neurosci. *19*, 163–171.

Dale, N., Hatz, S., Tian, F., and Llaudet, E. (2005). Listening to the brain: microelectrode biosensors for neurochemicals. Trends Biotechnol. *23*, 420–428.

Ding, F., O'Donnell, J., Thrane, A.S., Zeppenfeld, D., Kang, H., Xie, L., Wang, F., and Nedergaard, M. (2013). α1-Adrenergic receptors mediate coordinated Ca2+ signaling of cortical astrocytes in awake, behaving mice. Cell Calcium *54*, 387–394.

Duffy, A.M., Fitzgerald, M.L., Chan, J., Robinson, D.C., Milner, T.A., Mackie, K., and Pickel, V.M. (2011). Acetylcholine α7 nicotinic and dopamine D2 receptors are targeted to many of the same postsynaptic dendrites and astrocytes in the rodent prefrontal cortex. Synapse *65*, 1350–1367.

Freedman, R. (2014). α7-nicotinic acetylcholine receptor agonists for cognitive enhancement in schizophrenia. Annu. Rev. Med. *65*, 245–261.

Fujita, T., Chen, M.J., Li, B., Smith, N.A., Peng, W., Sun, W., Toner, M.J., Kress, B.T., Wang, L., Benraiss, A., et al. (2014). Neuronal transgene expression in dominant-negative SNARE mice. J. Neurosci. *34*, 16594–16604.

Fukushima, T., Kawai, J., Imai, K., and Toyo'oka, T. (2004). Simultaneous determination of D- and L-serine in rat brain microdialysis sample using a column-switching HPLC with fluorimetric detection. Biomed. Chromatogr. *18*, 813–819.

Gahring, L.C., Persiyanov, K., Dunn, D., Weiss, R., Meyer, E.L., and Rogers, S.W. (2004). Mouse strain-specific nicotinic acetylcholine receptor expression by inhibitory interneurons and astrocytes in the dorsal hippocampus. J. Comp. Neurol. *468*, 334–346.

Hashimoto, K., Fukushima, T., Shimizu, E., Komatsu, N., Watanabe, H., Shinoda, N., Nakazato, M., Kumakiri, C., Okada, S., Hasegawa, H., et al. (2003). Decreased serum levels of D-serine in patients with schizophrenia: evidence in support of the N-methyl-D-aspartate receptor hypofunction hypothesis of schizophrenia. Arch. Gen. Psychiatry *60*, 572–576.

Henneberger, C., Papouin, T., Oliet, S.H.H., and Rusakov, D.A. (2010). Long-term potentiation depends on release of D-serine from astrocytes. Nature *463*, 232–236.

Hernandez, C.M., Cortez, I., Gu, Z., Colón-Sáez, J.O.O., Lamb, P.W., Wakamiya, M., Yakel, J.L., and Dineley, K.T. (2014). Research tool: validation of floxed α7 nicotinic acetylcholine receptor conditional knockout mice using in vitro and in vivo approaches. J. Physiol. *592*, 3201–3214.

Hirase, H., Iwai, Y., Takata, N., Shinohara, Y., and Mishima, T. (2014). Volume transmission signalling via astrocytes. Philos. Trans. R. Soc. Lond. B Biol. Sci. *369*, 20130604.

Javitt, D.C. (2015). Current and emergent treatments for symptoms and neurocognitive impairment in schizophrenia. Curr. Treat. Options Psychiatry *1*, 107–120.

Johnson, J.W., and Ascher, P. (1987). Glycine potentiates the NMDA response in cultured mouse brain neurons. Nature *325*, 529–531.

Kantrowitz, J.T., Malhotra, A.K., Cornblatt, B., Silipo, G., Balla, A., Suckow, R.F., D'Souza, C., Saksa, J., Woods, S.W., and Javitt, D.C. (2010). High dose D-serine in the treatment of schizophrenia. Schizophr. Res. *121*, 125–130.

Kirkwood, A., Rozas, C., Kirkwood, J., Perez, F., and Bear, M.F. (1999). Modulation of long-term synaptic depression in visual cortex by acetylcholine and norepinephrine. J. Neurosci. *19*, 1599–1609.

Kleckner, N.W., and Dingledine, R. (1988). Requirement for glycine in activation of NMDA-receptors expressed in Xenopus oocytes. Science *241*, 835–837.

Kohtoh, S., Taguchi, Y., Matsumoto, N., Wada, M., Huang, Z.-L., and Urade, Y. (2008). Algorithm for sleep scoring in experimental animals based on fast Fourier transform power spectrum analysis of the electroencephalogram. Sleep Biol. Rhythms *6*, 163–171.

Labrie, V., Wong, A.H., and Roder, J.C. (2012). Contributions of the D-serine pathway to schizophrenia. Neuropharmacology *62*, 1484–1503.

Lee, M.G., Hassani, O.K., Alonso, A., and Jones, B.E. (2005). Cholinergic basal forebrain neurons burst with theta during waking and paradoxical sleep. J. Neurosci. *25*, 4365–4369.

Lin, H., Hsu, F.-C., Baumann, B.H., Coulter, D.A., and Lynch, D.R. (2014). Cortical synaptic NMDA receptor deficits in α7 nicotinic acetylcholine receptor gene deletion models: implications for neuropsychiatric diseases. Neurobiol. Dis. *63*, 129–140.

Ma, T.M., Abazyan, S., Abazyan, B., Nomura, J., Yang, C., Seshadri, S., Sawa, A., Snyder, S.H., and Pletnikov, M.V. (2013). Pathogenic disruption of DISC1-serine racemase binding elicits schizophrenia-like behavior via D-serine depletion. Mol. Psychiatry *18*, 557–567.

Maingret, N., Girardeau, G., Todorova, R., Goutierre, M., and Zugaro, M. (2016). Hippocampo-cortical coupling mediates memory consolidation during sleep. Nat. Neurosci. *19*, 959–964.

Markram, H., and Segal, M. (1990). Acetylcholine potentiates responses to N-methyl-D-aspartate in the rat hippocampus. Neurosci. Lett. *113*, 62–65.

Marrosu, F., Portas, C., Mascia, M.S., Casu, M.A., Fà, M., Giagheddu, M., Imperato, A., and Gessa, G.L. (1995). Microdialysis measurement of cortical and hippocampal acetylcholine release during sleep-wake cycle in freely moving cats. Brain Res. *671*, 329–332.

Martineau, M., Shi, T., Puyal, J., Knolhoff, A.M., Dulong, J., Gasnier, B., Klingauf, J., Sweedler, J.V., Jahn, R., and Mothet, J.-P. (2013). Storage and uptake of D-serine into astrocytic synaptic-like vesicles specify gliotransmission. J. Neurosci. *33*, 3413–3423.

Matus-Amat, P., Higgins, E.A., Sprunger, D., Wright-Hardesty, K., and Rudy, J.W. (2007). The role of dorsal hippocampus and basolateral amygdala NMDA receptors in the acquisition and retrieval of context and contextual fear memories. Behav. Neurosci. *121*, 721–731.

Moghaddam, B., and Javitt, D. (2012). From revolution to evolution: the glutamate hypothesis of schizophrenia and its implication for treatment. Neuropsychopharmacology *37*, 4–15.

Navarrete, M., Perea, G., Fernandez de Sevilla, D., Gómez-Gonzalo, M., Núñez, A., Martín, E.D., and Araque, A. (2012). Astrocytes mediate in vivo cholinergic-induced synaptic plasticity. PLoS Biol. *10*, e1001259.

Orozco-Ibarra, M., Medina-Campos, O.N., Sánchez-González, D.J., Martínez-Martínez, C.M., Floriano-Sánchez, E., Santamaría, A., Ramirez, V., Bobadilla, N.A., and Pedraza-Chaverri, J. (2007). Evaluation of oxidative stress in D-serine induced nephrotoxicity. Toxicology *229*, 123–135.

Panatier, A., Theodosis, D.T., Mothet, J.-P.P., Touquet, B., Pollegioni, L., Poulain, D.A., and Oliet, S.H.H. (2006). Glia-derived D-serine controls NMDA receptor activity and synaptic memory. Cell *125*, 775–784.

Paoletti, P., and Neyton, J. (2007). NMDA receptor subunits: function and pharmacology. Curr. Opin. Pharmacol. *7*, 39–47.

Paoletti, P., Bellone, C., and Zhou, Q. (2013). NMDA receptor subunit diversity: impact on receptor properties, synaptic plasticity and disease. Nat. Rev. Neurosci. *14*, 383–400.

Papouin, T., Ladépêche, L., Ruel, J., Sacchi, S., Labasque, M., Hanini, M., Groc, L., Pollegioni, L., Mothet, J.-P.P., and Oliet, S.H.H. (2012). Synaptic and extrasynaptic NMDA receptors are gated by different endogenous coagonists. Cell *150*, 633–646.

Pascual, O., Casper, K.B., Kubera, C., Zhang, J., Revilla-Sanchez, R., Sul, J.-Y., Takano, H., Moss, S.J., McCarthy, K., and Haydon, P.G. (2005). Astrocytic purinergic signaling coordinates synaptic networks. Science *310*, 113–116.

Paukert, M., Agarwal, A., Cha, J., Doze, V.A., Kang, J.U., and Bergles, D.E. (2014). Norepinephrine controls astroglial responsiveness to local circuit activity. Neuron *82*, 1263–1270.

Pinto, L., Goard, M.J., Estandian, D., Xu, M., Kwan, A.C., Lee, S.-H., Harrison, T.C., Feng, G., and Dan, Y. (2013). Fast modulation of visual perception by basal forebrain cholinergic neurons. Nat. Neurosci. *16*, 1857–1863.

Prickaerts, J., van Goethem, N.P., Chesworth, R., Shapiro, G., Boess, F.G., Methfessel, C., Reneerkens, O.A., Flood, D.G., Hilt, D., Gawryl, M., et al. (2012). EVP-6124, a novel and selective α7 nicotinic acetylcholine receptor partial agonist, improves memory performance by potentiating the acetylcholine response of α7 nicotinic acetylcholine receptors. Neuropharmacology *62*, 1099–1110.

Ripke, S., Neale, B., Corvin, A., Walters, J., Farh, K.-H., Holmans, P., Lee, P., Bulik-Sullivan, B., Collier, D., Huang, H., et al.; Schizophrenia Working Group of the Psychiatric Genomics Consortium (2014). Biological insights from 108 schizophrenia-associated genetic loci. Nature *511*, 421–427.

Schenberg, E.E., and Oliveira, M.G. (2008). Effects of pre or posttraining dorsal hippocampus D-AP5 injection on fear conditioning to tone, background, and foreground context. Hippocampus *18*, 1089–1093.

Schindelin, J., Arganda-Carreras, I., Frise, E., Kaynig, V., Longair, M., Pietzsch, T., Preibisch, S., Rueden, C., Saalfeld, S., Schmid, B., et al. (2012). Fiji: an open-source platform for biological-image analysis. Nat. Methods *9*, 676–682.

Schmitt, L.I., Sims, R.E., Dale, N., and Haydon, P.G. (2012). Wakefulness affects synaptic and network activity by increasing extracellular astrocyte-derived adenosine. J. Neurosci. *32*, 4417–4425.

Sharma, G., and Vijayaraghavan, S. (2001). Nicotinic cholinergic signaling in hippocampal astrocytes involves calcium-induced calcium release from intracellular stores. Proc. Natl. Acad. Sci. USA *98*, 4148–4153.

Shen, J.X., and Yakel, J.L. (2012). Functional α7 nicotinic ACh receptors on astrocytes in rat hippocampal CA1 slices. J. Mol. Neurosci. *48*, 14–21.

Shigetomi, E., Jackson-Weaver, O., Huckstepp, R.T., O'Dell, T.J., and Khakh, B.S. (2013). TRPA1 channels are regulators of astrocyte basal calcium levels and long-term potentiation via constitutive D-serine release. J. Neurosci. *33*, 10143–10153.

Singh, N.S., Paul, R.K., Ramamoorthy, A., Torjman, M.C., Moaddel, R., Bernier, M., and Wainer, I.W. (2013). Nicotinic acetylcholine receptor antagonists alter the function and expression of serine racemase in PC-12 and 1321N1 cells. Cell. Signal. *25*, 2634–2645.

Su, M., Hu, H., Lee, Y., d'Azzo, A., Messing, A., and Brenner, M. (2004). Expression specificity of GFAP transgenes. Neurochem. Res. *29*, 2075–2093.

Sultan, S., Li, L., Moss, J., Petrelli, F., Cassé, F., Gebara, E., Lopatar, J., Pfrieger, F.W., Bezzi, P., Bischofberger, J., and Toni, N. (2015). Synaptic integration of adult-born hippocampal neurons is locally controlled by astrocytes. Neuron *88*, 957–972.

Takata, N., Mishima, T., Hisatsune, C., Nagai, T., Ebisui, E., Mikoshiba, K., and Hirase, H. (2011). Astrocyte calcium signaling transforms cholinergic modulation to cortical plasticity in vivo. J. Neurosci. *31*, 18155–18165.

Teles-Grilo Ruivo, L.M., and Mellor, J.R. (2013). Cholinergic modulation of hippocampal network function. Front. Synaptic Neurosci. *5*, 2.

Vardjan, N., Parpura, V., and Zorec, R. (2016). Loose excitation-secretion coupling in astrocytes. Glia *64*, 655–667.

Vecsey, C.G., Wimmer, M.E., Havekes, R., Park, A.J., Perron, I.J., Meerlo, P., and Abel, T. (2013). Daily acclimation handling does not affect hippocampal long-term potentiation or cause chronic sleep deprivation in mice. Sleep *36*, 601–607.

Wolosker, H., and Radzishevsky, I. (2013). The serine shuttle between glia and neurons: implications for neurotransmission and neurodegeneration. Biochem. Soc. Trans. *41*, 1546–1550.

Yang, Y., Paspalas, C.D., Jin, L.E., Picciotto, M.R., Arnsten, A.F., and Wang, M. (2013). Nicotinic α7 receptors enhance NMDA cognitive circuits in dorsolateral prefrontal cortex. Proc. Natl. Acad. Sci. USA *110*, 12078–12083.

Zant, J.C., Kim, T., Prokai, L., Szarka, S., McNally, J., McKenna, J.T., Shukla, C., Yang, C., Kalinchuk, A.V., McCarley, R.W., et al. (2016). Cholinergic neurons in the basal forebrain promote wakefulness by actions on neighboring non-cholinergic neurons: an opto-dialysis study. J. Neurosci. *36*, 2057–2067.

Zappettini, S., Grilli, M., Olivero, G., Chen, J., Padolecchia, C., Pittaluga, A., Tomé, A.R., Cunha, R.A., and Marchi, M. (2014). Nicotinic α7 receptor activation selectively potentiates the function of NMDA receptors in glutamatergic terminals of the nucleus accumbens. Front. Cell. Neurosci. *8*, 332.

Zhang, Y., Chen, K., Sloan, S.A., Bennett, M.L., Scholze, A.R., O'Keeffe, S., Phatnani, H.P., Guarnieri, P., Caneda, C., Ruderisch, N., et al. (2014). An RNA-sequencing transcriptome and splicing database of glia, neurons, and vascular cells of the cerebral cortex. J. Neurosci. *34*, 11929–11947.

Zhao, S., Ting, J.T., Atallah, H.E., Qiu, L., Tan, J., Gloss, B., Augustine, G.J., Deisseroth, K., Luo, M., Graybiel, A.M., and Feng, G. (2011). Cell type–specific channelrhodopsin-2 transgenic mice for optogenetic dissection of neural circuitry function. Nat. Methods *8*, 745–752.

STAR★METHODS

KEY RESOURCES TABLE

REAGENT or RESOURCE	SOURCE	IDENTIFIER
Antibodies		
Rabbit polyclonal anti-GFP	Invitrogen	Cat. No. A11122; RRID: AB_221569
Goat polyclonal anti-ChAT	Millipore	Cat. No. AB144P; RRID: AB_2079751
Chicken polyclonal anti-GFAP	Abcam	Cat. No. AB4674; RRID: AB_304558
Rabbit polyclonal anti-NeuN	Millipore	Cat. No. ABN78; RRID: AB_10807945
Bacterial and Virus Strains		
AAV2/5-GFAP(0.7)-eGFP-T2A-iCre	Vector Biolabs	Cat. No. VB1131
AAV2/9-eSYN-eGFP-T2A-iCre	Vector Biolabs	Cat. No. VB1089
Chemicals, Peptides, and Recombinant Proteins		
Encenicline (EVP-6124)	MedChem Express	Cat. No. HY15430A; CAS: 550999-74-1
L-Norepinephrine	Santa Cruz	Cat. No. SC-279253; CAS: 329-56-6
Adenosine	Sigma-Aldrich	Cat. No. A9251; CAS: 58-61-7
Atropine	Sigma-Aldrich	Cat. No. A0257, CAS: 5908-99-6
CPT (8-cyclopentyl-1 3-dimethylxanthine)	Sigma-Aldrich	Cat. No. C102; CAS: 35873-49-5
D-serine	Sigma-Aldrich	Cat. No. S4250; CAS: 312-84-5
L-serine	Sigma-Aldrich	Cat. No. S4500; CAS: 56-45-1
Methoxamine hydrochloride	Sigma-Aldrich	Cat. No. M6524; CAS: 61-16-5
Picrotoxin	Sigma-Aldrich	Cat. No. P1675; CAS: 124-87-8
Tricine	Sigma-Aldrich	Cat. No. T0377; CAS: 5704-04-1
$ZnCl_2$	Sigma-Aldrich	Cat. No. 211273; CAS: 7646-85-7
AR-R17779 hydrochloride	Tocris	Cat. No. 3964; CAS: 178419-42-6
Carbamylcholine	Tocris	Cat. No. 2810; CAS: 51-83-2
DhβE (Dihydro-β-erythroidine hydrobromide)	Tocris	Cat. No. 2319; CAS: 29734-68-7
MLA (Methyllycaconitine citrate)	Tocris	Cat. No. 1029; CAS: 112825-05-5
NBQX disodium salt	Tocris	Cat. No. 1044; CAS: 479347-86-9
PPADS tetrasodium salt	Tocris	Cat. No. 0625; CAS: 192575-19-2
Ro25-6981 maleate	Tocris	Cat. No. 1594; CAS: 1312991-76-6
SCH 442416	Tocris	Cat. No. 2465; CAS: 316173-57-6
Critical Commercial Assays		
D-serine biosensor Sarissaprobe	Sarissa Biomedical	Cat. No. SBS-DSER-05-50
Null biosensor Sarissaprobe	Sarissa Biomedical	Cat. No. SBS-NUL-05-50
Pierce BCA Protein Assay Kit	Thermo Fisher	Cat. No. 23225
Experimental Models: Organisms/Strains		
Mouse: ChAT-ChR2-eYFP (B6.Cg-Tg(Chat-COP4*H134R/EYFP,Slc18a3)6Gfng/J)	The Jackson Laboratory	Jax No.: 014546
Mouse: dnSNARE (GFAP-tTA:TeTO-dnSNARE)	Pascual et al., 2005	Available upon request
Mouse: α7nAChR^{flox} (B6(Cg)-Chrna7tm1.1Ehs/YakelJ)	Hernandez et al., 2014; Jackson laboratory	Jax No.: 026965
Oligonucleotides		
Primer: Exon 4 Chrna7 Forward: GTGCCAGACCACATGT GCATTGG	This paper	N/A
Primer: Exon 4 Chrna7 Reverse: GGTCACTGAGCAGTG GTGGACAG	This paper	N/A
Primer: ChAT-ChR2-eYFP transgene Forward: TCTGTT CCCAGGTCGGCAGC	Zhao et al., 2011	N/A

(*Continued on next page*)

Continued

REAGENT or RESOURCE	SOURCE	IDENTIFIER
Primer: ChAT-ChR2-eYFP transgene Reverse: GCAAGGTAG AGCATAGAGGG	Zhao et al., 2011	N/A
Primer: dnSNARE TSL transgene Forward: TGGATAAAGAAG CTCATTAATTGTCA	Pascual et al., 2005	N/A
Primer: dnSNARE TSL transgene Reverse: GCGGATCCAG ACATGATAAGA	Pascual et al., 2005	N/A
Primer: dnSNARE tTA transgene Forward: ACTCAGCGCT GTGGGGCATT	Pascual et al., 2005	N/A
Primer: dnSNARE tTA transgene Reverse: GGCTGTACGCG GACCCACTT	Pascual et al., 2005	N/A
Software and Algorithms		
Fiji	Schindelin et al., 2012	https://fiji.sc/
SleepSign	Kissei Comtec	http://www.sleepsign.com/
Freeze Frame and Freeze View	Coulbourn Instruments	http://www.coulbourn.com/category_s/277.htm
Clampex 9.2 and Clampfit9.2	Molecular Devices	N/A
Other		
Accucore C18 column for HPLC	Thermo Fisher	Cat. No. 17126-152130
Micro-dialysis probe	Harvard Apparatus	Cat. No. CMA 7 P000082
Guide Cannula	Harvard Apparatus	Cat. No. CMA P000138

CONTACT FOR REAGENT AND RESOURCE SHARING

Further information and requests for resources and reagents should be directed to and will be fulfilled by the Lead Contact, Philip Haydon (philip.haydon@tufts.edu).

EXPERIMENTAL MODEL AND SUBJECT DETAILS

All animal experiments were conducted in accordance with the guideline of the Animal Care and Use Committee of Tufts University.

Animals, housing and genotyping

Adult male mice (3-6 months old) were used throughout this study with the exception of Figure 7 where experiments were occasionally performed on α7nAChR$^{flox/flox}$ or α7nAChR$^{+/+}$ females. All animals were kept on a 12-12 light-dark cycle and housed in groups of 2-5 siblings with water and food ad libitum. No mouse was single-housed for more than 24h under any circumstances, including after surgery where littermates were housed back together as soon as sternal recumbency was reached. Behavior and electrophysiology experiments were conducted by a male experimenter. Littermates of the same sex were randomly assigned to experimental groups.

ChAT-ChR2-eYFP BAC transgenic mice were purchased from Jackson Laboratory (*B6.Cg-Tg(Chat-COP4*H134R/EYFP)6Gfng/J*, Stock #014546) and bred in our facility (2 females and 2 males founders). Genotyping was performed on tails samples taken from 7 day old pups using the same set of primers and PCR cycling conditions described in Zhao et al. (2011). Mice referred to as ChAT-ChR2-eYFP$^{-/-}$ (or ChR2$^{-/-}$) were littermate non-carriers of the transgene.

Heterozygous α7nAChR$^{floxed/+}$ mice in which exon 4 of the *Chrna7* gene is flanked by loxP sites (*B6-Chrna7*^{LBDEx4007Ehs}) originated from Dr. K. Dineley's lab (Department of Neurology, University of Texas, Medical Branch, Galveston, TX 77555) where they were generated as described in Hernandez et al. (2014). They were cleared from quarantine after 2 weeks, backcrossed with C57BL/6 mice and bred in our facility. Primers used for genotyping were: (forward) GTG CCA GAC CAC ATG TGC ATT GG and (reverse) GGT CAC TGA GCA GTG GTG GAC AG, giving a 474 base pair (bp) band for the endogenous *Chrna7* allele and a ~650bp band for the floxed allele (see Figure S7).

The dnSNARE mice were bred and genotyped as previously described (Pascual et al., 2005; Sultan et al., 2015). In these mice, the expression of the tetracycline transactivator (tTA) is driven by the *GFAP* promoter, which ensures the selective expression of the construct in astrocytes of adult mice. In the absence of Doxycycline (Dox), tTA binds to the tetracycline response element which permits the expression of the dnSNARE and eGFP transgenes. The dnSNARE transgene codes for the cytosolic portion (96 amino acids) of the vesicle associated membrane protein VAMP2 which acts as a dominant-negative that inhibits vesicular exocytosis (Sultan et al., 2015). Importantly, breeders were maintained on a Dox-containing diet (40mg/kg) at all times and pups (all genotypes) were kept on Dox until they were weaned (4 weeks), in order to prevent in utero and developmental expression of the transgene. This is of paramount

importance since *GFAP* promotor activity, although selectively restricted to astrocytes in adults (see Zhang et al., 2014; http://web.stanford.edu/group/barres_lab/cgi-bin/igv_cgi_2.py?lname=gfap), is found in a population of neuronal precursor cells during early post-natal development (Su et al., 2004). GFAP-tTA negative mice were used as single gene controls (Figure 4). Animals were used 8 weeks after Dox removal from diet. Additionally, 12 dnSNARE mice were put back on a Dox-containing diet at ~P80 for 4 weeks before being used for electrophysiology (Figure 4) in order to shut off transgene expression and control for possible off-target long-lasting cellular effects of dnSNARE expression ("dnSNARE on Dox"). Importantly, some doubts have been raised by Fujita et al. (2014) about the cell-selectivity of the expression of the dnSNARE construct in these mice. In their publication, they reported broad and marked expression of the transgene GFP reporter in hippocampal and cortical neurons. This is not the case for the dnSNARE line originating from and bred in our lab and we encourage readers to refer to Figure S3 where we performed immunohistochemistry and extensive cell counting that demonstrate the absence of neuronal expression of the transgene in our line. In particular we show that not a single eGFP-positive neuron was found among 5,884 and 5,887 neurons counted (by two separate investigators) in confocal z stacks of images taken from dnSNARE off Dox mice from our lab (See section on Immunohistochemistry, fluorescence imaging and cell counting, below). This is in agreement with all but one publication that have used dnSNARE mice since they were generated in 2005, and in strikingly contrasts with results from Fujita et al., suggesting possible genetic drift of the line used by Fujita et al. or technical/procedural issues in their study (such as the absence of Dox during development).

Zeitgeber timescale

The Zeitgeber time (ZT) scale arbitrarily sets the origin of the 24h period (ZT0) to the onset of the light-phase, allowing comparison among studies independently of the actual clock-time settings of animal facilities. Onset of light (ZT0) was at 7am during daylight saving time and 6am otherwise in our facility. It should be noted that for electrophysiology experiments at ZT0, mice that were still awake in their home cage at that time were favored over mice already nested. This criterion was applied to avoid mitigating effects due to periods of rest of unknown duration prior to light onset. We measured that an average of 3 min elapsed between taking the mouse cage off the rack in the animal facility to the decapitation of the animal.

METHOD DETAILS

Slice preparation

Experiments were carried out on acute hippocampal slices from adult male mice (3-6 months). After decapitation under isoflurane anesthesia, the brain was quickly removed from the skull and placed in ice-cold artificial cerebrospinal fluid (aCSF) saturated with 95% O_2 and 5% CO_2 and containing 2mM Mg^{2+} and 1mM Ca^{2+} to limit excitotoxicity. Hippocampal coronal slices (350 μm) were incubated 35 min at 33°C in 1.5 mM Mg^{2+} and 2 mM Ca^{2+}-containing aCSF and then allowed to recover for 45 min at room temperature. Slices were then transferred into a recording chamber, where they were perfused with aCSF (~1 mL/min) saturated with 95% O_2/5% CO_2. The aCSF composition was (in mM): 125 NaCl, 2.5 KCl, 1.25 NaH_2PO_4, 26 $NaHCO_3$ and 10 glucose (pH 7.3, 290-300 $mOsm.L^{-1}$).

Field recordings

Schaffer collaterals were electrically stimulated at 0.05 Hz with a concentric tungsten electrode placed in the *stratum radiatum*. Evoked field excitatory post-synaptic potentials (fEPSPs) were recorded using a glass electrode (2-4 MΩ) filled with aCSF and placed in the *stratum radiatum*. Intensity of stimulation (< 120 μA, 100 μs, except for Figure S5A, where a different stimulator was used) was set appropriately to avoid population spikes, and the slope of field responses was monitored throughout. Experiments were performed at 33°C in the presence of 2 mM Ca^{2+} and 50 μM picrotoxin. NMDAR-mediated responses were isolated in low Mg^{2+} concentration (0.2 mM) with 10 μM NBQX to block AMPA/Kainate receptors. When AMPAR-mediated responses were recorded (Figure S5), NBQX was omitted and the concentration of Mg^{2+} was 1.3 mM. Data were recorded with an Axopatch C (Axon Instruments), and collected and analyzed using Clampex9.2 and Clampfit9.2 software (Axon Instruments). Average traces were obtained from 20-30 min of stable recordings. Unless major run-up, rundown or electrical noise appeared on the recordings that prevented accurate analysis, no experiments were excluded.

Optogenetics

For ChR_2 excitation in slices from ChAT-ChR2-eYFP BAC transgenic mice, square pulses of blue light (460/50 nm, 20 ms duration) were delivered through the 40X water immersion objective of a Prairie Technologies Uncager microscope equipped with a 75 W mercury lamp (Olympus, U-LH75XEAPO). Illumination was applied to the entire visual field centered on the tip of the recording pipette and the output light power measured at the microscope objective was 600-800 μW. Trains of light-pulses were delivered using a high-speed shutter (Uniblitz VMM-D4, Vincent Associates). The frequency and duration of trains (5 Hz, 10sec) were controlled by an A310 Accupulser (World Precision Instruments) triggered by Clampex9.2. When brain slices were obtained from ChAT-ChR2-eYFP BAC transgenic mice, care was taken to reduce exposure to light during the slicing procedure and when slices were manipulated under the microscope.

Drugs

With the exception of EVP-6124 hydrochloride (MedChem Express) that was injected i.p. at 0.4 mg/kg, drugs were purchased from Tocris or Sigma, prepared as 1000X aliquots (stored at −20°C) in distilled water, DMSO (CPT) or 90% alcohol (picrotoxin) and bath

applied at concentrations indicated in the main text with a 1:1000 dilution. D-serine was also injected i.p. at 200mg/kg for behavioral experiments. $ZnCl_2$ 250 nM (Sigma) was used in 10 mM Tricine (Sigma) with the relation $[Zinc]_{free} = [Zinc]_{applied}/200$ (Paoletti and Neyton, 2007; Papouin et al., 2012). It should be noted that Zinc and Ro25-6981 are partial antagonists that inhibit ~70%–80% and ~90% of the current flowing through GluN2A-NMDARs (GluN1/GluN1/GluN2A/GluN2A) and GluN2B-NMDARs (GluN1/GluN1/GluN2B/GluN2B), respectively (Paoletti and Neyton, 2007). The subunit composition of NMDARs impacts many of their properties and in particular their affinity for glycine and D-serine (Paoletti et al., 2013), and remains unchanged throughout the 24h period in our study guarantees that their affinity for exogenous D-serine is unchanged.

EVP-6124 (or vehicle: 0.04% DMSO in saline) was injected i.p. at ZT0 in awake mice (9 mice total for this experiment), in the animal facility. Mice were then immediately returned to their home cage with their siblings and left undisturbed for 4 hr (ZT4). During this time, they were closely monitored to check for possible behavioral effects of EVP-6124 injection. All of the 9 injected mice nested and were immobile in the hour following the injection. None of the mice injected with EVP-6124 showed any sign of prolonged wakefulness or enhanced locomotor activity (see below).

D-serine biosensor measurements in conditioned medium

For D-serine measurements with amperometric biosensors, slices were obtained exactly as described above for electrophysiology experiments. Typically, 6-8 hemi-slices were obtained for those experiments, approximately spanning from Bregma −1.5 to −2.6. After 30min at 33°C and 45min recovery at RT, slices were taken individually to carefully separate the hippocampus from the rest of the slice. To minimize manipulation and damage to slices, a small portion of cortex immediately above the hippocampus (motor and somatosensory cortex typically) was left attached and therefore participated in the following incubation. Hippocampal-cortical slices were then allowed an additional 15min of recovery before being placed in 3mL of aCSF gently oxygenated with 95% O_2/5% CO_2, where they were incubated for 90min at RT. Ca^{2+} and Mg^{2+} concentration were 2mM and 1.5mM respectively. To favor oxygenation and access to glucose, this incubation was performed in two separate 1.5 mL tubes that received 3-4 hippocampal slices each. The conditioned medium (CM) was then carefully drained and immediately frozen (−80°C) until used for D-serine measurement (see below). Incubated tissue was frozen too (−80°C) until protein extraction was performed using a Pierce BCA protein assay kit. On average, the concentration of protein for all incubated 6-8 slices was, in WT: 13.8 ± 0.7 mg/ml of protein at ZT0 and 13.1 ± 0.4 mg/mL at ZT6; and in dnSNARE: 10.1 ± 0.8 mg/ml of protein at ZT0 and 12.7 ± 0.8 mg/ml of protein at ZT6. Two CM measurements fell under the detection limit of our sensors, raising uncertainties about their accuracy, and were excluded from the analysis (Figure 4F).

D-serine and null biosensor electrodes, 0.5 mm in length and 50-60 μm in diameter, were purchased from Sarissa Biomedical and used according to manufacturer's instructions (Dale et al., 2005; http://www.sarissa-biomedical.com/products/sarissaprobes.aspx). These biosensors consist of platinum electrodes coated with D-serine degrading enzyme (DAAO) embedded in a perm-selective layer (the null-sensor consisting of the perm-selective layer alone is used to subtract non-selective signals). The degradation of D-serine by DAAO involves the stoichiometric use of 2 electrons, which provides a linear electronic readout of D-serine concentration. Calibration experiments showed that the biosensor electrodes reliably and linearly detect D-serine for concentrations of 0.1 to 50 μM (Figure 1), in line with manufacturer specifications. The electrodes were mounted on Scientifica micromanipulators to allow submersion and positioning in the recording chamber of the electrophysiology setup at 33°C in a vehicle solution (aCSF made the day of slice incubation). Control of biosensors' potential and measurement of current through biosensors were operated using a bipotentiostat (Digi-IVY, Model DY2023). Biosensors and null sensors were rehydrated at 33°C for 30 min to 1h under continuous perfusion of the vehicle solution. Cycling from −500 to +500 mV and back was carried out several times as suggested by manufacturer, and biosensors were then allowed to polarize to +500 mV for 60 min until capacitive decay was imperceptible. The CM was then perfused in the recording chamber where the biosensors were submerged. The aCSF made on the day of CM collection was used as the baseline and wash-out vehicle solution. The volume of CM incubated with slices (3 mL) was set by preliminary experiments aimed at determining the minimal volume of CM allowing plateau detection by the biosensors with this method. As seen on traces of Figure 1F, artifacts usually appeared on recordings as the perfusion system was switched to the CM or from the CM back to the vehicle solution (after the 3 mL had passed through). A similar artifact was purposefully generated during perfusion of the calibrating (1 μM) D-serine solution when 3 mL had passed through, by gently tapping the recording chamber. As can be seen on the calibration trace (Figure 1F, bottom) the plateau detection is fully reached by the time 3 mL have been perfused (artifact on the trace). Though no current was generally observed on the null-sensor, currents measured on this sensor electrode were subtracted from currents measured on the D-serine sensor electrode to obtain a pure "D-serine-induced" amperometric signal. Sensors were calibrated at the end of every experiment with 0.1, 0.5, 1 and 10 μM D-serine to measure their sensitivity (in our hands, some biosensor electrodes successfully detected D-serine amounts as low as 50 nM). This allowed a determination of the absolute concentration of D-serine in CM.

Classical use of these biosensors consists of penetrating brain slices with the biosensor electrode itself, which typically results in an immediate peak detection of tens of μM of D-serine, likely due to tissue destruction and irreversible damage to neurons and glia, causing intracellular D-serine (which accounts for most of brain D-serine) to be released into the extracellular space. After tens of minutes of decay this is expected to stabilize to a steady-state level thought to reflect the endogenous extracellular concentration of D-serine in slices (Shigetomi et al., 2013). Instead, this is more likely to reflect residual amounts of D-serine escaping the scarring/dying tissue surrounding the biosensor. Additionally this approach is highly dependent on how deep sensors are forced into the slice, which dictates how much of the sensor is in contact with damaged tissue and therefore how much D-serine is detected.

Last but not least, we found that such a method could cause deterioration of the sensor itself upon penetration in the slice. Together these concerns encouraged us to employ a different approach (conditioned medium approach), described above.

Enforced-wakefulness and enriched-environment housing

Enforced-wakefulness (EW) is usually achieved by ''gentle handling'' which consists of exposing animals to unknown and potentially stressful stimulations for about 6 hr (new bedding, new cage, handling, novel objects, noise and poking, rattling on the cage grid) (Vecsey et al., 2013). In an effort to achieve EW with minimal stress to the animals, EW was carried out over a shorter duration and without handling at all. Since D-serine availability decreases within the first hour of the light-phase (Figure 1) we were able to assess the effect of only 2 hr of EW. This is still sufficient to distinguish between a circadian and a wakefulness-dependent mechanism (see main text) while avoiding any confounding effects from long periods of EW that increase locomotor activity and cause stress as shown by dramatic elevation of corticosterone levels (Vecsey et al., 2013). This also allowed EW to occur in home cages without handling the mice, removing the bedding, grid, water or food and without presentation of any novel object. The cage was simply placed in a new room. Typically, no further action was required to maintain animals awake for the first hour since this was enough to elicit classic exploratory behavior and social interaction. For the following hour, the cage was occasionally gently displaced to maintain the animals alert and by 1.5h into the EW, the filter-lid was partially removed from the top of the cage. Subsequent olfactory stimulation provided enough arousal to keep mice awake until ZT2.

Enriched environment housing (EEH) consisted of novel objects such as plastic hamster tunnels, igloos, cubes, slides and platforms of different colors and textures dispersed around the cage (objects were wiped with alcohol beforehand). Items were not fixed to the bottom of the cage and mice were free to displace them. Three to five males from the same litter were housed in the same, large cage (26 × 47 × 20 cm). The grid was removed and the cage top was covered with high-ceiling lid so that mice could also explore their environment vertically. Food was provided ad libitum and water was provided via two 40 mL water dispensers (BioServInc #9019), also contributing to novelty. Finally, at the onset of the dark-phase (ZT12), mice were provided a running metallic wheel that was removed at the onset of the light-phase (ZT0). EEH was provided for at least 2 consecutive days and limited to a maximum of 5 days in order to prevent habituation.

In vivo microdialysis and HPLC

Cannula implantation: 6-8 week old male C57BL/6J mice (Jackson Laboratory, 000664) received a unilateral cannula implantation surgery. Briefly, mice were anesthetized using isoflurane. Buprenorphine (0.05mg/kg, sub cutaneous) was given pre-operative and post-operative as needed. Hippocampal coordinates were measured (−2mm, left 1.5mm) from Bregma and the midline. The guide cannula (CMA P000138) was inserted just above the cortex and secured with dental cement and two contra lateral anchor screws. Mice recovered 7 days before sampling. Cannula implantation was verified at the end of the experiments following transcardiac 4% PFA perfusion and brain sectioning. Placement of the cannula was assessed by a separate investigator and animals showing mistargetting were excluded from the HPLC analysis. All procedures were approved by Tufts IACUC. *Microdialysis*: Mice were habituated to single housing for at least 7 days prior to sampling. On the day of sampling, probes (CMA P000082) were inserted through the guide cannula at ZT0. ACSF (Harvard Appparatus, 597316) was perfused through the probe at a rate of 0.5ul/minute for 6 hr. Dialysis samples were collected every hour and frozen at −80C. During sampling, mice were video recorded using Pinnacle video capture software. *Video scoring*: Animals were scored as active (mobile or immobile but awake) or inactive (nested and absence of movement) each minute of the 6 hr recording. The average activity over the 6 hr sampling was then compared to the average concentration of D-serine collected in the dialysis sample. *High performance liquid chromatography*: D-serine detection was performed using HPLC and an Accucore C18 column (Thermo Fisher, 17126-152130). An organic phase (methanol) and aqueous phase (50mM phosphate buffer, pH 4.34) were perfused at a rate of 200ul/minute in a step protocol: 0-6 min 3% organic, 6.5-10 min 20% organic, 11-14 min 80% organic, and equilibrated at 3% organic for 7 min. Samples were diluted in half with aqueous mobile phase and derivatized using o-Phthaldialdehyde (Pickering, O120) and N-Acetyl-L-Cysteine (Sigma, A8199). After derivatization, 1M acetic acid was added. 1ul of sample was injected and run on the column, followed by a second replicate run from the same sample. Standards were prepared from D- and L-serine (Sigma) in aqueous mobile phase at a ratio of 1:10. The area under the D-serine peak was used to calculate the sample concentration relative to standards. For each animal, the average activity was plotted versus the average D-serine concentration. Statistical significance was assessed using a correlation analysis.

Wakefulness assessment, EEG-EMG recordings and analysis

The implantation of electroencephalogram (EEG) electrodes (Pinnacle Technology) was conducted stereotaxically under isoflurane anesthesia on 6-8 week old male C57BL/6J mice (Jackson Laboratory, 000664). The skull surface was exposed and four insulated wire electrodes were placed and screwed as follows: two extradural cortical electrodes were inserted bilaterally in the frontal areas and the other two were inserted bilaterally in the parietal areas. Two insulated wire electrodes were inserted bilaterally into the nuchal muscle for electromyogram (EMG) recordings. Electrodes connected to a micro-connector (Pinnacle technology) were secured at the surface of the skull with dental acrylic. Mice received buprenorphine (0.08 mg/kg) and saline i.p. and allowed 5 days of recovery. Lightweight recording cables (Pinnacle Technology) were connected to the head implants and mice were placed in Pinnacle Plexiglas cages containing water and food ad libitum for acclimation for 2-3 days. EEG and EMG signals were amplified and bandpass filtered at 0.5–100 Hz and 10–100 Hz, respectively, using a 15 LT Bipolar Physiodata amplifier system (Grass Technologies) and sampled at

400 Hz with a MP150 data acquisition system (BIOPAC Systems). The system was equipped with infra-red cameras to monitor mice behavior and activity throughout the recording. EEG and EMG waveforms were then analyzed as in Kohtoh et al. (2008) using SleepSign for Animal software (Kissei Comtec) with minor changes. Briefly, waveforms were analyzed by 10 s epochs (1024 FFT points). Each Epoch was divided in 5 regions that were FFT calculated with a Hanning Window and averaged. Three frequency bands were calculated: δ (0.75-4Hz), θ (4-8Hz) and α (8-12Hz) and the values were used to determine vigilance states using the following algorithm with the indicated order of priority: 1-Clear locomotion or EEG integral > 3-5 μV/sec = active wakefulness; 2- EEG integral < 3-5 μV/sec and EEG δ power > 250-500 μV^2 = Non-REM sleep; 3- EEG integral < 3-5 μV/sec and EEG θ/(δ+ θ) ratio and/or EEG α /(δ+ α) > 45% = Non-REM sleep; 4- otherwise = quiet wakefulness. For experiments in which mice were administered saline or EVP-6124 i.p. (Figure 5), their activity was assessed in home cage for the following 4hrs through video monitoring and scored by minute bins as in Figure 2 (score 1: wakefulness, locomotor activity or otherwise active behavior; score 0: immobility).

Fear conditioning

All mice used for behavior were exclusively handled by a male investigator (TP) who also performed cage change over the few weeks prior to experiments. Here again, mice were fully adult (3 to 6 months old) and housed in groups of 2-5. We measured that an average of 2 min elapsed between the time the mouse cage was taken off the rack in the facility to moment animals were all placed in the 4 fear conditioning chambers (i.e., 5min or less until first shock). Mice were naive, had undergone no previous procedure (except for i.p. injections where applicable, see below) and were sacrificed within 24h after the training session. Mice that were used for fear conditioning were not re-used for electrophysiology or any other type or procedures or experiments. Out of 155 animals used for fear conditioning experiments, only 3 were excluded from the analysis for the following reasons: blindness, escaping the fear enclosure, impaired baseline locomotor and exploratory behavior.

Four conditioning chambers (Coulbourn Instruments, H10-11R-TC) were situated inside a sound-attenuating isolation cabinet (Coulbourn Instruments, H10-24T). They consisted of metal rod floors, two metallic walls, one of which was mounted with a dim ceiling-facing white light bulb, a metallic ceiling, a rear plexiglass panel and a front plexiglass opening. Grid floor was connected to a precision shocker (Coulbourn Instruments H13-15) administering 0.5mA, 2 s shocks. The tray, grid floor, ceiling and all four wall panels of the chamber, as well as the inside of the sound-attenuating cabinet were thoroughly wiped with 70% alcohol solution and dried before and after each session. A Panasonic WV-BP334 B/W camera was mounted in the celling of each chamber connected to a PCI-1410 (ACT-610) interface, allowing subsequent automated detection and measurement of freezing responses using FreezeFrame and FreezeView software (Coulbourn Instruments). Freezing was defined as a complete and continuous absence of movement, except for respiratory motion, for at least 1 s.

Training consisted of a single 5min session during which two shocks were delivered (at t = 180 and 240 s). No auditory stimuli were provided. Mice were then immediately placed back in their home cage and returned to the animal facility. Testing was carried out 24h later for all groups, except for acquisition/short-term memory assessment that was performed 1h after training (Figure 3E). Testing consisted of a single session of 3 min during which no shocks were delivered. Context B consisted of visual, olfactory, tactile, dimensional and lighting differences to context A. It was obtained by using a small plastic enclosure (17 cm wide X 27 cm long X 17 cm high) with a distinctive plastic smell, positioned in the center of the original conditioning chamber. Its walls were high enough to mask the rest of the conditioning chamber and covered with a black and white checkered motif. The floor of the enclosure was padded with lab diapers to mask the underlying grid floor. Diapers texture was new to mice and very distinctive from the metallic rods through which the shocks were delivered during training. Brighter lighting was provided. No auditory stimulus was presented in either context. For the ZT23 group, handling of mice was carried out under red light, except for the dim lighting of the contextual chamber. Mice were returned to the animal facility at least 30min prior to light onset.

For D-serine administration experiments, littermates were randomly separated into receiving a different treatment and run simultaneously. Brain extracellular D-serine concentration peaks ~1 hr after i.p. D-serine injection and lasted at least 1h (Fukushima et al., 2004). D-serine (200 mg/kg) and vehicle (0.9% saline) were therefore injected i.p. into wild-type littermates 1h prior to conducting behavior training. This dose of D-serine was efficient at increasing extracellular brain D-serine, as shown by micro-dialysis measurements (Figure S3B). The 1h delay between injection and training also prevented cueing the training with the unpleasant injection procedure.

Adeno-associated viruses and stereotaxic surgeries

Two to three month old mice from the $\alpha 7nAChR^{floxed}$ line were anesthetized by isoflurane inhalation. Buprenorphine HCl (0.1 mg/kg) was administered subcutaneously as a pre-emptive analgesic. Once under deep anesthesia, mice were immobilized in a Kopf stereotaxic apparatus using intra-aural positioning studs to stabilize the skull and a hole was drilled on the surface of the skull at the appropriate coordinates. Using a 30G needle and Neuros syringe (Hamilton Co.), 2 μL of AAV5-GFAP(0.7)-eGFP-T2A-iCre (2.6×10^{10} genome copies, Vector Biolabs #VB1131) were injected into area CA1 with the following coordinates (anterior, lateral, depth [mm] relative to Bregma): (−2.0, +1.5, −1.5) or 1 μL of AAV9-eSYN-eGFP-T2A-iCre (7.8×10^9 genome copies, Vector Biosystems #VB1089) into the CA1 and CA3 areas: (−2.0, +1.5, −1.5) and (−2.0, +2.6, −2.2) respectively. Injection rates of 100 nL/min were controlled by a micro syringe pump controller (World Precision Instrument Micro4). After injection, the incision site was sutured with 6-0 nylon sutures (Unify, #XS-N618R11). Animals were postoperatively monitored until recovered.

Recordings were obtained from slices of AAV5-GFAP(0.7)-eGFP-T2A-iCre or AAV9-eSYN-eGFP-T2A-iCre injected $a7nAChR^{flox/flox}$ animals or $\alpha 7nAChR^{+/+}$ littermates at three different ZT times (see main text). eGFP fluorescence in slices was visualized under 460 nm

light, and recording and stimulating electrodes were placed accordingly in regions of interest (ROI) of the CA1 *s. radiatum* with the best levels of fluorescence. Immediately after recordings, slices were briefly mounted on a slide and the location, spread and penetrance (% fluorescent cells) of the infection was inspected by appreciating the eGFP fluorescence under an epifluorescence microscope. For the AAV9-injected animals, the infection was considered successful when eGFP fluorescence was observed both in CA3 and CA1 pyramidal neurons, including cell bodies, dendrites and Schaffer collaterals. Transduction failures in either of these regions typically resulted in the cell bodies not being fluorescent (despite strong fluorescence in surrounding layers due to projections from transduced regions). Results from slices showing no or low infection in either CA3 or CA1 were discarded from the final analysis. For either virus serotype, results from slices showing no transduction at all were pooled and considered as "sham" (ie, surgery/injection controls) in Figure 7L.

Immunohistochemistry, fluorescence imaging and cell counting

Mice were anesthetized with isoflurane then transcardially perfused with PBS followed by 4% paraformaldehyde (PFA). Brains were extracted, post-fixed and cryoprotected by immersion in 30% (w/v) sucrose in PBS at 4°C. Brains were sectioned (50 μm thick) using a sliding microtome (Leica SM2000R). Sections were washed with PBS containing 0.3% Triton X-100 (PBS-Tx), and non-specific labeling was blocked using 5% bovine serum albumin (BSA). Sections were incubated with primary antibodies diluted in 1% BSA/0.3% Tx in PBS overnight at 4°C on an orbital shaker. The following primary antibodies were used: anti-GFP (1:1000, Invitrogen, A11122), anti-ChAT (1:200, Millipore, AB144P), anti-NeuN (1:1000, Millipore, ABN78), and anti-GFAP (1:1000, AbCam, ab4674). The following day, sections were washed three times in PBS-Tx then incubated with the appropriate AlexaFluor 488, 594, 633 secondary antibody (1:1000, Life Technologies) for 2 hr at room temperature on an orbital shaker. After the incubation, sections were rinsed with PBS-Tx three times then mounted on Superfrost Plus slides (VWR) and coverslipped with Vectashield HardSet Mounting Medium with DAPI (Vector Laboratories). Whole section imaging was performed using the 10x lens of a Keyence BZ-X710 fluorescence microscope. Confocal stacks were taken using a Nikon A1R confocal microscope equipped with a 20x (N.A. 0.75) and 40x oil-immersion lens (NA 1.0). Images were acquired with a resolution of 1024 × 1024 pixels. Images were adjusted for brightness and contrast in Fiji (Schindelin et al., 2012). Anti-GFP and anti-ChAT immunostaining in Figure 6 was performed as in Zhao et al. (2011). Sections from dnSNARE mice were immunostained with anti-GFAP and anti-NeuN.

Cell counting in Figures 7 and S4 was performed independently by two investigators (TP and JD) on at least 12 high-resolution z stacks (3 animals, 2 sections per animal, 2 stacks per section) spanning the 50 μm range of tissue at 1-2 μm increments. The Cell Counter plug-in in Fiji (Schindelin et al., 2012) was used to colocalize each cell's nucleus (DAPI staining) with a cell-specific marker (GFAP or NeuN) and the reporter (GFP) by scanning through the z-planes manually. In results shown in Figures 7B–7D and 7I–7K, both the AAV5 virus and the AAV9 virus were remarkably selective for astrocytes and neurons respectively. For the AAV5 virus, we found that 100% (investigator 1, JD) and 99.8% (investigator 2, TJP) of eGFP expressing cells (1271 and 1174 eGFP+ cells counted respectively; 90-100 cells per stack) were GFAP+ (i.e., astrocytes). On average 80.0 ± 2.0% (JD) and 80.4 ± 3.0% (TJP) of all astrocytes (GFAP+) in the ROI (total astrocytes JD: 1592, TJP: 1467) were eGFP+ (expressing iCre). In sections from AAV9 injected mice, we found that virtually all eGFP+ cells in area CA1 and 98 to 99% of eGFP+ cells in CA3 were NeuN+ (i.e., neurons) and that ~75% of all neurons (JD: 73.4 ± 5%; TJP: 78.8 ± %6%) in the ROI expressed iCre recombinase (eGFP+).

QUANTIFICATION AND STATISTICAL ANALYSIS

When applicable (field recordings, D-serine biosensor measurements in conditioned medium, in vivo micro-dialysis and HPLC, fear conditioning, adeno-associated viruses and stereotaxic surgeries), exclusion criteria are explained in the corresponding method section above. Briefly, no electrophysiology experiments were excluded unless major rundown, run-up or noise prevented accurate analysis. Two C.M. measurements were excluded from the analysis because they fell under the biosensors detection limit. Only 3 out of 155 animals were excluded in the fear conditioning experiments due to blindness, lack of locomotor activity or escaping the enclosure. Finally, viral infections and micro-dialysis probes were excluded in case of lack of infection and/or mistargetting. In all electrophysiology experiments, n indicates the number of independent slices analyzed. In behavior experiments, n indicates the number of independent animals. For in vivo micro-dialysis/HPLC experiments, n indicates the number of animals from which one dialysate was obtained. For fluorescence imaging, n is the number of individual cells counted. This information is explicitly reported in all figures either as a number in the bar graph or as individual data points. An analysis of variance was performed with a Shapiro-Wilk normality test to verify normality of data distribution whenever applicable and determine the appropriate subsequent statistical analysis. Statistical tests used in this study are paired or unpaired Student's t tests, Pearson tests, an agreement test, a Wilcoxon Matched-pairs signed rank test, and one-way or repeated-measures ANOVAs followed, whenever appropriate, by Bonferroni post hoc tests. Statistical tests used are reported in figure legends and/or in the text along with the n-value, the test-value (F(df1, df2), *t*(df) etc…) and the exact p value. P value of 0.05 was used as the significance threshold throughout this study. When statistical results are reported for a group of comparisons using the same test, the test-value is omitted and the closest p value is reported. In figures, p values are illustrated as follow, for all tests used: $p > 0.05$: n.s.; $p < 0.05$: *; $p < 0.01$, **; $p < 0.001$: ***.